PFC/RR-83-20 DOE/ET/51013-91

12 T Solenoid Design Options for the MFTF-B Upgrade

by Joel H. Schultz and Nikolai Diatchenko

Fusion Engineering Design Center

M.I.T. Plasma Fusion Center Report PFC/RR-83-19

July 29, 1983

12 T Solenoid Design Options for the MFTF-B Upgrade

by Joel H. Schultz and Nikolai Diatchenko

Fusion Engineering Design Center

M.I.T. Plasma Fusion Center Report PFC/RR-

July 25, 1983

1. Introduction

The Lawrence Livermore Laboratory is planning an upgrade of the MFTF-B tandem mirror facility that will include enhanced plasma physics performance, along with the possiblity of doing nuclear component testing in a central cell. The first design concept considered for this upgrade was labelled MFTF-B+T, in honor of the tritium fuel. In the original concept, the central nuclear testing volume was surrounded by two high field solenoids, which allowed high plasma density in the nuclear testing area, as shown in Figure 1. These solenoids are required to provide a field on axis of 12 T, of which 2-3 T would be provided by background solenoids. The 12 T coils were physically close to the nuclear testing area, requiring possible neutron and gamma shielding to protect the magnets.

The major options for the 12 T magnets examined here are the selection of normal, superconducting or hybrid normal/superconducting magnet systems. The tradeoffs are those between the higher initial cost of superconducting magnet system, the need for thick shielding of superconducting magnets, higher recirculating power in the normal magnets and poorly characterized reliability of lightly shielded normal magnets. The size and shielding tradeoffs among these options are illustrated in Fig. 2.

The design concepts presented here are evaluated only for the first design iteration of MFTF-B+T, mentioned above. In particular, all concepts now being considered have made topological improvements in the center cell, so that neutral beam power is no longer a strong function of choke coil size. This function was strongly favorable to the use of normal magnets over superconducting magnets and its absence will be discussed qualitatively in the cost comparisons.

2. Normal Magnets

Two options for normal magnets are considered: an organically insulated, wound magnet and an inorganically insulated Bitter plate magnet. Both designs have positively retained insulation, in the belief that highly irradiated insulation will crack, but may be able to survive electrical stresses in a design with sufficiently low voltage. Both designs are also constrained to operate at terminal voltages less than 100 V, in the belief that the electrochemical destruction mechanisms in highly irradiated magnets require both electric field and high irradiation. However, this constraint leads to very high current magnets whose bus and power supply requirements will partially cancel the normal magnet's cost advantage over superconducting alternatives.

2.1 Wound normal magnet concept

A wound normal magnet concept, using organic insulation, was developed for the all normal option. The normal magnet design is shown in Figures 3-6. Its major parameters are listed in Table I. The magnet has a peak field at the magnet of 12.3 T, 7.46 MAT in the winding and an overall current density in the winding pack of 2 kA/cm^2. The total electrical power required for the two magnet power conditioning and cooling circuits is 17.7 MW. The magnet is wound with 48 turns in two double pancakes with 12 layers per pancake, as shown in Figure 3. The conductor concept resembles that of the TF magnets in JET, as shown in Figure 4. This conductor was selected because it is the largest known conductor with two internal cooling holes. It thus lends itself to the high current/low voltage design needed for the intense irradiation environment, while containing the recirculating water in a internally cooled concept that does not permit any contact between water and insulation.

The cooling requirements of the coil are set by the need not to degrade the insulation properties or to anneal copper. The cooling concept selected was to feed each turn from a top header and return at the bottom of each turn through a bottom header, as shown in Figure 5. This concept allows cooling of an internally cooled magnet with temperature rises comparable to those achievable with external cooing. A variation on this concept is used below for cooling the Bitter plate magnet concept.

The high current joint concept is shown for the connection of the two pairs of parallel leads to the bus. The joints are soldered with redundant shear pins, as is done in the normal magnet joints in Doublet III. Mechanical rigidity is provided by by 6 high strength bolts for each of the six joints. All insulation is fully retained, by a

steel case around the joint region, since the joints are made in a region with significant neutron and gamma irradiation.

2.2 Bitter plate normal magnet concept

The Bitter magnet design is shown in Figures 7-14. The normal Bitter magnet with ceramic insulation is sized as the insert coil in a hybrid magnet system. The background superconducting coil is of the same topology (two grades, Nb_3Sn, internally cabled, externally cooled) as the all superconducting choke system discussed below in the next section. In the hybrid magnet system, the normal insert magnet provides 5.0 T of the field on axis. 5.0 T is provided by the superconducting background coils and the remaining 2.0 T by the rest of the solenoid system. The rest of the tandem mirror system is moved back self-consistently in these designs by taking account of the space requirements of the center cell beamline. This is the reason why the contribution of the rest of the system to the 12 T under the choke coil is smaller for the two options with superconducting magnets than for the all normal magnet. The overall dimensions of the hybrid system are shown in Figure 7. The Bitter magnet insert provides 4.05 MAT with an overall current density of 1.32 kA/cm^2 and a recirculating power of 5.2 MW.

A more detailed view of the Bitter magnet is shown along with the background coil case in Figure 8. There are 26 plates in the magnets, with staggered electrical and hybraulic crossovers brazed from one plate to another. Current is returned through the case, so that current leads can leave on one side of the magnet in a coaxial strip,to avoid fringe fields in the plasma. It this feature is unnecessary, it would be easier to construct the magnet with a high side and low side lead, with no return through the case.

The internally cooled Bitter magnet concept has the short cooling paths of an externally cooled magnet design, while containing the water out of contact with the ceramic insulation. This magnet is considerably more complex than a conventional Bitter magnet, because of the requirement that the ceramic must be positively contained everywhere. While the complexity of the design suggests the posiibility of improvements in the design concept, this design is, to the best of our knowledge, the only concept that has been defined for a high irradiation, high field magnet, in which the insulation is retained everywhere, including the leads.

Neither the wound nor the Bitter magnet approach the ideal of constant stress polyhelical design. This is not necessary for a 12 T magnet, but will become more necessary for an 18 T magnet, such as those used as plug

magnets at the ends of the split central solenoid. The ideal polyhelical design should allow somewhat higher fields, if a design solution can be found to retaining the insulation.

Figure 9 illustrates the internal joint concept, which is perhpas the most unique feature of the Bitter plate magnet design. A crossover piece is prebrazed to the inner plate. The outer plate is laid over the crossover piece and brazed to it. A sleeve, not shown, would be used to prevent braze material from entering the hydraulic coolant channel, and for alignment of the plates. The crossover piece is shown as being initially welded from two pieces, one of which may require final adjustments before welding for coolant hole alignment. As shown, the crossovers, as well as the plates are surrounded by tightly packed sheets of ceramic insulation, which is in turn surrounded by a steel jacket.

The Bitter plate internal cooling channel concept is shown in Figure 10. Water enters the plate from a small internal header within the magnet case and exits after flowing through half a turn into a header at the bottom. On the crossover side of the plate, water must flow into the adjacent plate in order to reach the bottom header at the end of a half turn. Figure 11 shows the internal header connections to the Bitter plate cooling channels. The header is insulated by ceramic powder from the Bitter plates.

Figure 12 shows the range of positions of the internal crossovers between Bitter magnet plates. Crossovers begin at the bottom side of the magnet at the leads and move upward a plate thickness at every turn until the far side of the magnet. The build is sufficiently low, however, that the crossovers can be stacked horizontally, without requiring radial crossovers, which would be far more difficult. The internal cooling channels in the crossover bars are also shown in Figure 12.

Figure 13 illustrates the leads with fully retained insulation. Each lead has its own insulation and sheath about it. Since the return lead has been taken on two sides from the magnet case, it begins as a double lead surrounding the forward lead, forming a flat shield about the forward lead and producing negligible radial field in the plasma. This design answers the concerns about whether leads can be designed that are structurally well contained. The open lead configuration of the theoretically more efficient polyhelical design appears to be a likely source of magnet failure under intense irradiation.

Figure 14 shows the coolant penetration to the internal header. The internal header region is filled with ceramic powder, since there are too many small radius bends to permit laying ceramic sheets in this region. The feedthrough in this case is imagined to be an organic/fibreglass composite, but with ceramic sheet insulation between the structural piece through which the hydraulic line is fed through and the coil case. In a design

without return currents through the case, both pieces could be grounded.

2.3 Discussion

Three fundamental assumptions, based on our previous work in the area of highly irradiated, high stress magnets [SC82], have driven the design thought behind the two normal magnet alternatives:

1 Any design with water in contact with an organic insulation will fail rapidly. Any design with water in direct contact with an inorganic insulation is highly suspect.

2 All insulation, whether organic or inorganic, must be positively retained everywhere. Under intense irradiation, bonds will fail and insulation will crack and/or powder. The only mechanically reliable insulation design is one where the insulation has nowhere to go. This eliminates designs with solid, ceramic spacers, no matter how high their yield strength or how low their swelling under irradiation may be.

3 Any magnet depending on strong, ductile materials for its mechanical strength will last a while before neutron embrittlement ultimately destroys it. The rapid failure mechanisms - erosion, corrosion, photolysis, electrolysis, photoconductivity and tracking - are electrochemical in their nature and are catalyzed by the presence of electric field. Therefore, we have imposed as a design rule that the terminal voltge of the normal magnets must be lower than 100 V. This leads to high current leads, bus and power supplies which are considerably more expensive than a higher voltage design would be.

The Bitter magnet design was developed in the most detail in the belief that it might be the simplest solution to the definition of an internally cooled magnet with fully retained insulation. However, an examination of the relative complexities of the Bitter and wound magnets does not really support this conclusion. The wound magnet is indeed very close to the ideal of having its insulation completely retained and appears to be less complex than the Bitter magnet. This is a reversal of the usual experience at high field magnet laboratories at which a Bitter magnet typically costs an order of magnitude less than a wound coil with similar performance, but the additional complexity required to prevent water contact with the insulation and to retain the insulation is considerable, as illustrated in the drawings.

In both sets of drawings, the insulation is sufficiently contained that there is nothing that clearly indicates whether the insulation must be organic or inorganic. The insulation compressive fatigue tests by Becker, in particular, under intense irradiation cast considerable doubt on previous interpretations of the allowable radiation doses on organic insulations. These tests suggest that thin sheets of composite organic/inorganic materials,

such as G-10, have enormously high lifetimes in compression, presumably because they have nowhere to go. However, this optimistic assessment of the organic insulations in highly irradiated environments is balanced against the ambiguous operating experience of highly irradiated magnets in accelerator laboratories, which have included massive failures of magnets with organic insulation at DESY, as well as very high lifetimes elsewhere, and against the knowledge that the domimant failure mechanism may be electrical and chemical, rather than purely structural. Thus the need for field experience is clearly indicated, preferably with both organic and insulation alternatives. The need to select a particular organic or inorganic insulating material appears to be less important, although there is good reason to believe that polyimides with S-glass fillers should have radiation life.

The discussion above has been a roundabout approach to the following conclusions:

1 A modification of the wound magnet alternative appears to be somewhat more attractive than the Bitter magnet option. This modification would be in the direction of fully retaining the insulation.

2 If budgetary constraints permit, it would be beneficial to the D & T requirements of the mirror program to build one of the normal choke magnets with organic insulation, such as a polyimide resin with an S-glass filler, and one with inorganic insulation, such as spinel, magnesia or alumina. The relatively low integrated fluence of MFTF-B+T, in comparison with a mirror reactor, means that considerably less downtime would be associated with the incorporation of this technology experiment with the overall objectives of the machine than if field experience were postponed to a later machine.

3. Superconducting Magnet

The superconducting magnet option, also used in the sizing of the hybrid magnet below, is the Airco Nb_3Sn, internally cabled conductor, used in the Westinghouse LCP and M.I.T./Livermore 12 T coils. The Airco conductor was selected because of familiarity with it as an advanced superconductor. However, more advanced conductors, such as the internal tin Nb_3Sn of IGC or the already developed 15 kA Nb_3Sn ICS conductor of Showa will also be considered.

The dimensions of the all superconducting magnet choke system are shown in Figure 15. The key parameters of the system are shown in Table I. The overall winding pack has an inner radius of 0.58 m and and an outer radius of 1.18 m and a length of 1.4 m. The superconducting choke coil contributes 9.9 T to the total 12 T field on axis. The maximum field at the superconductor is 13.1 T. The superconducting coil requires

17.9 MAT with an overall current density over the winding pack of 2.05 kA/cm^2. The winding pack shape was selected to minimize the winding pack volume for a desired field on axis, with R_1 fixed. This is undoubtedly not an optimal geometry for a graded superconductor with a strong field dependence of conductor current on field in the high field grade. The algorithm for selecting the layer at which grading would take place accepted the fixed overall dimensions and minimized the total amount of noncopper, designing to a fixed fraction of critical current. Another weakness in this algorithm, is that it scaled the field with the layer number, because it was written before an exact calculation of self and external fields in each layer had been incorporated into the system model. Using this algorithm, the minimum superconductor volume happened to be such that the low current/high field grade carried almost exactly half the current of the high current/low field grade. Thus, it was decided to make the ratio exactly half, in order to allow a single lead pair to provide current to both grades. A more sophisticated algorithm for shape selection will be developed in the future.

The magnet cooling concept is the externally-cooled, cable-in-conduit concept adopted for the TF magnets of Alcator DCT, which avoids the high cryogenic entropy generation associated with internal, force-flow cooling. This concept is illustrated in Figure 16. In this concept, neutron and gamma losses are removed by conduction to a small pool of boiling helium. The ICS conductors have a void fraction of 40 % helium, in order to absorb sudden energy depositions in the winding during energization. The conductors are wound in double pancakes and are sealed on both ends. The pool between double pancakes can be subcooled, in order to allow higher critical currents. This concept is scheduled to be tested in the Fall of 1983 by the M.I.T./Livermore ICS 12 T coil.

The critical current selection is based largely on the experimental work of Hoenig and Steeves [HO82]. It is believed that the critical current at 13 T will be improved over that implied by the Westinghouse LCP Final Design Report [WE80] because of two factors: the coils will be reacted after they are wound and the void fraction of the conduits will be larger. The dominant strain in these magnets should be compressive due to cool-down from the reaction temperature to cryogenic temperatures. The well-known strain-dependence of Nb_3Sn is illustrated in Figure 17, in which an interpretation of the experimental data in Figure 18 is superimposed on the curves published in the Westinghouse LCP Design Report. As can be seen (with difficulty), the curve of actual strain at 12 T vs. void fraction generated by Hoenig lies exactly on top of the curve of critical current vs. tensile strain measured by Westinghouse. Figure 17 shows that, at 12 T the critical current is about a third higher at 40 % void fraction than at 32 %. The dashed curve on the bottom represents the expected performance of the

Westinghouse LCP coil at 12 T. The additional degradation in critical current is because of the increase in the peak compressive strain in the conductor due to bending during winding after reacting. Although Hoenig's data does not include the design value of 13.1 T, it does include tests at 15 T, so the projected value for the MFTF-B application is based on interpolation.

4.0 Stress Analysis

A simple stress analysis was done, assuming that the conductor is self-supporting radially and that layers are unbonded and supported in compression against a stiff case on one end. The axial stress profiles for hoop tension and axial compression are shown in Figures 19-35 for the normal, superconducting and hybrid coils.

The total axial and radial field in a normal magnet of the wound normal magnet choke system is shown in Figures 19, 20 and 21. For all coils, the fields will be illustrated for a turn in the outer layer, center layer, and inner layer of the winding pack as a continuous function of axial position. This is, of course, somewhat idealized, since the the Bitter magnet has no layers, the wound coil has an even number of layers and all concepts are discrete axially. However, the purpose of this calculation is to gain insight into the mechanical integrity of the three concepts with a model which is sufficiently sophisticated to model the effect of the actual, asymmetric force field, without modeling about hopefully second-order effects, which remain a topic for future work. The self, external and total axial field of the inner, high field layer of the normal choke is shown in Figure 20. In this particular option, the asymmetry in the axial field is not very high. The radial field, however, is almost equal in all layers, fairly high (up to 3.5 T) and antisymmetric about the coil axial center plane.

The axial stresses in the normal choke coil are shown in Figure 22. The worst spot among those analyzed is in the center layer near the axial center plane, with a compressive bearing stress of -15.4 MPa. Stresses are everywhere negative, indicating that each layer is attracted to the axial center plane of the mirror reactor. Since the stress decreases toward the low-Z side, the Lorentz forces on the low-Z pancake must be away from machine center, but it is forced against the inside wall by the other pancakes.

The hoop stresses in the normal choke coil are shown in Figure 23. The maximum stress analyzed is 81 MPa in the center layer, near the axial center plane of the coil. The combined hoop and axial stress results in a Tresca stress of 96 MPa near the center of the normal coil. If the filling factor of copper in the wound coil is 85 %, the hoop stress would be 95 MPa and the Tresca stress 110 MPa. This would be below an allowable of about 150 MPa for half-hard copper, implying that steel strip reinforcement may not be necessary.

The axial and radial fields in the all superconducting choke magnet system are shown in Figures 24-26. The self, external and total axial field are shown in Figure 25, showing little asymmetry, as was observed for the normal choke coil. The radial field is higher for the superconducting coil than for the normal coil, with a maximum value of 5.2 T. The radial field is also nearly the same for all layers and nearly antisymmetric.

The hoop stress in the superconducting coil has a maximum of 200 MPa near the center of the inner layer, as shown in Figure 27 The maximum axial stress of 39 MPa is in the center layer. An allowable bearing stress of 130 MPa would allow a fairly high stress multiplier in the inter-double pancake pool boiling channels. The peak Tresca stress of 232 MPa in the inner layer, averaged over a conductor envelope, compares with an allowable of about 170 MPa in 1/4 hard copper at 4 K and 540 MPa in the JBK-75 sheath, if 1/3 of ultimate tensile strength is used. This could be marginally covered by the reference design, in which 45 % of the envelope is copper or Nb_3Sn (= 77 MPa, average) and 30 % is JBK-75 (= 180 MPa, average). Reduction of the peak stress, if necessary could be achieved by taking the contribution of the cold case into account, by adding steel strip or by thickening the conduit wall.

The axial and radial fields in the superconducting and normal coils in the hybrid system are shown in Figures 29-31. The radial field in the normal coil is reduced by about 50 % from its value in the all normal choke coil. The radial field vs. axial position of the superconducting coil is now highly asymmetric, reaching a peak of 3.12 MPa about a third of the way down the coil, axially, as shown in Figure 31.

The hoop stress in the superconducting coil is reduced by nearly a factor of two, almost proportional to the reduction in field contribution, in the superconducting coil from what it was in the all superconducting choke system. The stress peaks towards the machine center at 117 MPa. It also peaks towards machine center for the other layers. The axial stress in the superconducting coil is reduced even more to a maximum bearing stress at the machine center side of -12.9 MPa, as shown in Figure 33. The maximum Tresca stress is now 129 MPa, which is well within the allowable stress levels of the reference ICS conductor.

The hoop stress in the normal magnet is highest in the outer layer, peaking at 52 MPa near the axial center of the magnet, as shown in Figure 34. The axial stress is more nearly constant than in the stand-alone design and peaks near the center. The outer layer is pushed away from the machine axis, while the inner layer is pulled toward it. It is not surprising that the fringe fields might be significantly different in a hybrid magnet in which the insert coil has a significantly smaller axial extent than the background magnet, than in a stand-alone solenoid. However, the qualitatively different behavior of the hybrid magnets indicates a need to calibrate

the numerical solutions obtained here against results from a second method. This is now being done with the implementation of a three-dimensional, closed-form solution to solenoid stresses being developed by Bobrov.

The peak Tresca stress in the normal magnet in a hybrid choke system is approximately 58 MPa. Thus it appears that the stresses in the hybrid choke system have significantly higher safety margins than in either the normal or superconducting choke system. The superconducting coil would have 2.5 times the stress level of the all normal coil and would be marginal with either a pure copper or with the current form factor of the high strength steel (JBK-75) sheath of the present Westinghouse LCP conductor. The stress allowable, however, would be higher for the superconducting magnet than for the normal magnet because of the lower temperature and lighter irradiation level.

The stress analysis above cannot be considered to be definitive, since a number of other important factors must be considered in order to obtain the true stresses. In particular, the hydraulic channels in the normal magnet designs remove about half of the axial bearing surface in the vicinity of the fittings, doubling the axial stresses in those regions. Similarly, the bubble-clearing channels in the superconducting coil have the same effect. On the other hand, the assumption that the windings must be self-supporting is conservative, since the cases or cowound structural strips can be used to increase the conductor strength. The interpretation of these preliminary stress analyses is that all three of these concepts are likely to have high stresses in the conductors, but that all three appear to be feasible. The highest safety margins appear to be in the hybrid magnet. A possible reason is that the sizing algorithm, which minimized volume in the superconducting magnets and recirculating power in the copper magnets probably has a bias toward more structurally conservative designs in hybrid magnets.

5.0 Cost Trade Study

The relative system costs were estimated for the normal, superconducting and hybrid magnet systems. No attempt was made to identify cost differences between the wound and Bitter normal concepts. A weakness of this analysis is that the authors are not intimately familiar with the MFTF facility at Livermore. This is particularly important when attempting to develop a realistic estimate of the cost auxiliary systems. This defect should be corrected in the next design iteration. The costs of the various subsystems for the normal choke option are shown in Figures 36-38. The costs of the various sybsystems for the superconducting choke option are shown in Figures 39-41. The costs of the various sybsystems for the hybrid choke option are shown in Figures

42-45. In every case, the largest subsystem cost is that of the neutral beam systems. Much of this cost, however, is independent of the selection of the choke magnet system. The neutral beam system is estimated to be $5.7 M less expensive for the normal choke system than for the hybrid system and $6.9 M less expensive than for the superconducting choke system. This is larger than the differential cost of the magnets, including their auxiliary systems. The normal magnet system was estimated to cost $3 M less than the hybrid magnet system and $2.9 M less than the superconducting magnet system. The conclusion was that the normal magnet system was significantly less expensive than the hybrid and superconducting systems, which both had approximately the same price. This conclusion would still hold, if the dependence of neutral beam system cost on magnet dimensions were dropped.

With the linear dependence of beam power on incremental magnet length from machine center, the tradeoff between capital and operating costs appears to be weighted in favor of minimizing capital costs, because the additional neutral beam power in the case of the superconducting alternatives cancels much of the Joule heating in the copper magnets. The peak line power was lowest for the all superconducting choke system at 58.7 MW, which was lower than that in the hybrid system by 3.9 MW and lower than that in the normal magnet system by 10 MW. This led to a differential utility charge, using rate structures provided by Pacific Gas and Electric, of $70 K per year less for the superconducting magnet than for the hybrid and $200 K per year less for the superconducting magnet than for the normal coil. This corresponds to approximately a 15 year return on investment in the comparison of the normal coil with the superconducting coil for the magnet system costs only, and a 50 year return on investment, if the differential in neutral beam heating costs are included. This tradeoff may change drastically in the next iteration, if there is no magnet size penalty related to auxiliary heating, or if the duty cycle of the machine is increased. However, when the desire to minimize capital costs is added to the desire to obtain some field experience with highly irradiated normal magnets, the first tradeoff iteration favored the use of normal choke magnets to produce 12 T on axis.

Acknowledgments

This work was done under the overall supervision of B. Hunter and S. Kalsi at the Magnetics Group at the Fusion Engineering Design Center. Drawings and machine system integration was provided by J. O'Toole at the Design Center. The authors would like to thank D.B. Montgomery and R.J. Thome for useful discussions.

References

[HO82] M.O. Hoenig and M.M. Steeves, "Experimental parameter study of subsize Nb_3Sn cable-in-conduit conductors," Applied Superconductivity Conference, Knoxville, TN, Dec 1982

[SC82] J.H. Schultz, "Design Practice and Operational Experience of Highly Irradiated, High Performance Normal Magnets," M.I.T. Plasma Fusion Center Report PFC/RR-82-25, Sept. 1982

[WE80] Westinghouse Electric Corp, "Superconducting magnet coils for the Large Coil Program, Phase 2 Final report to Union Carbide Corporation, Volume 1: Introduction and verification testing report," Mar 31, 1980

Table I

Performance Specifications of Three 12 T Magnet Options

Parameter	Normal	Superconducting	Hybrid Normal	Hybrid Superconducting
B_o, field on axis (T)	12	12	12	12
B_o, choke coil (T)	9.3	9.9	5.0	5.0
(choke contribution)				
B_{max}, magnet (T)	12.3	13.1	12.5	6.34
Ampere-turns (MAT)	7.46	17.9	4.05	9.37
λJ (A/m^2)	20.0	20.5	13.2	18.2
R_1 (m)	0.16	0.58	0.16	0.723
R_2 (m)	0.61	1.18	0.63	1.13
Z_1 (m)	2.55	2.85	3.08	2.98
Z_2 (m)	3.23	4.25	3.82	3.92
t_{shield}	0.0	0.4	0.0	0.59

Table II

Cost Figures of Three 12 T Magnet Options

Option	I Normal Normal	II Superconducting Superconducting	III - Hybrid Normal	III - Hybrid Superconducting
	(M$)	(M$)	(M$)	(M$)
Neutral Beam System	46.5	53.4	52.2	-
Magnet System	4.67	7.56	2.65	5.06
Magnet Shield	0.0	0.24	0.0	0.18
Total	55.8	69.0	68.0	

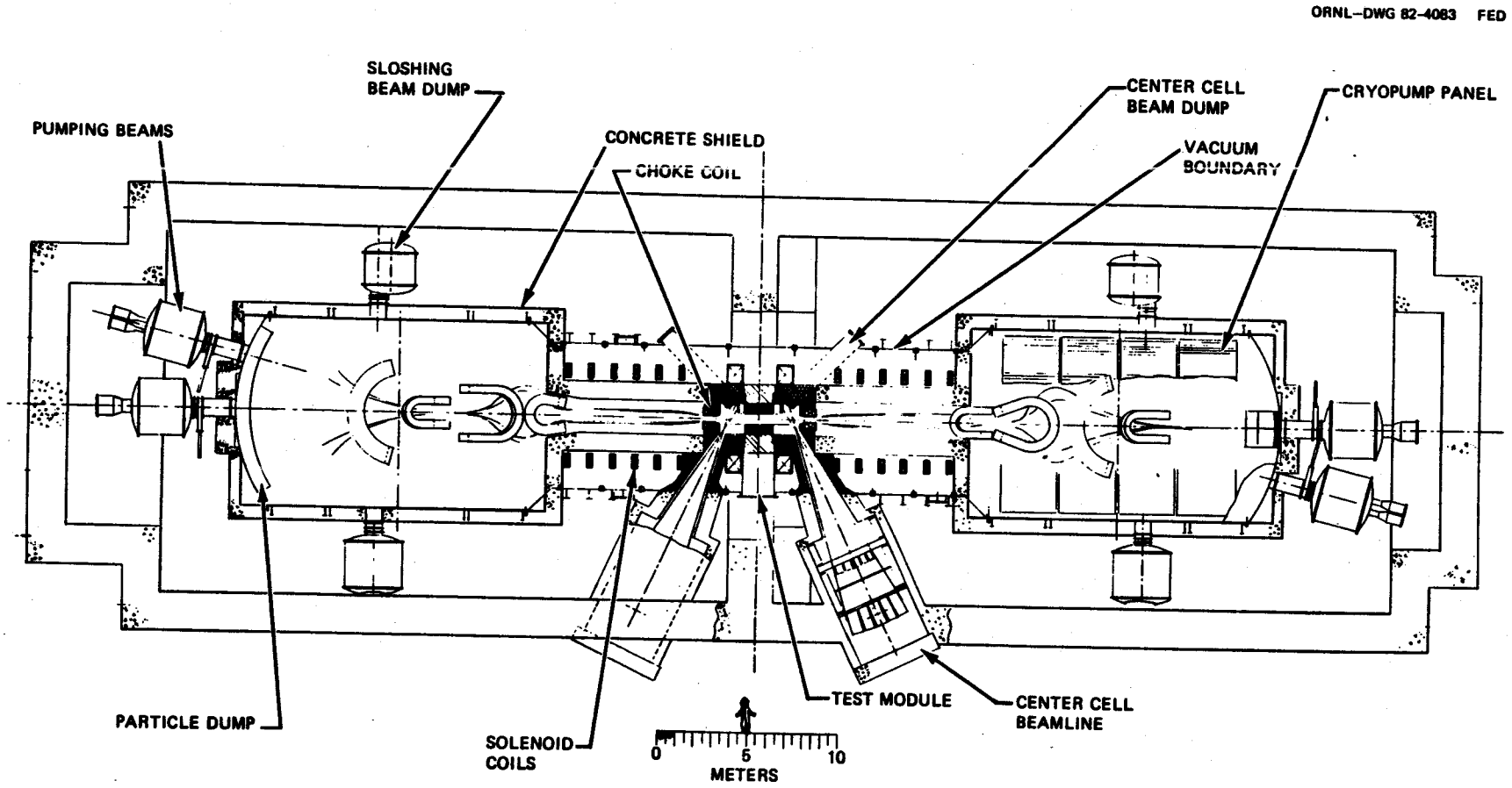

MFTF-B+T CONFIGURATION

FOR CLARITY COMPONENTS SHOWN ROTATED INTO PLAN OF PAPER

DECEMBER 16, 1982

(COURTESY OF THE FUSION ENGINEERING DESIGN CENTER)

FIGURE 1

CONFIGURATION STUDY

SUPERCONDUCTING vs RESISTIVE CHOKE COIL

(COURTESY OF THE FUSION ENGINEERING DESIGN CENTER)

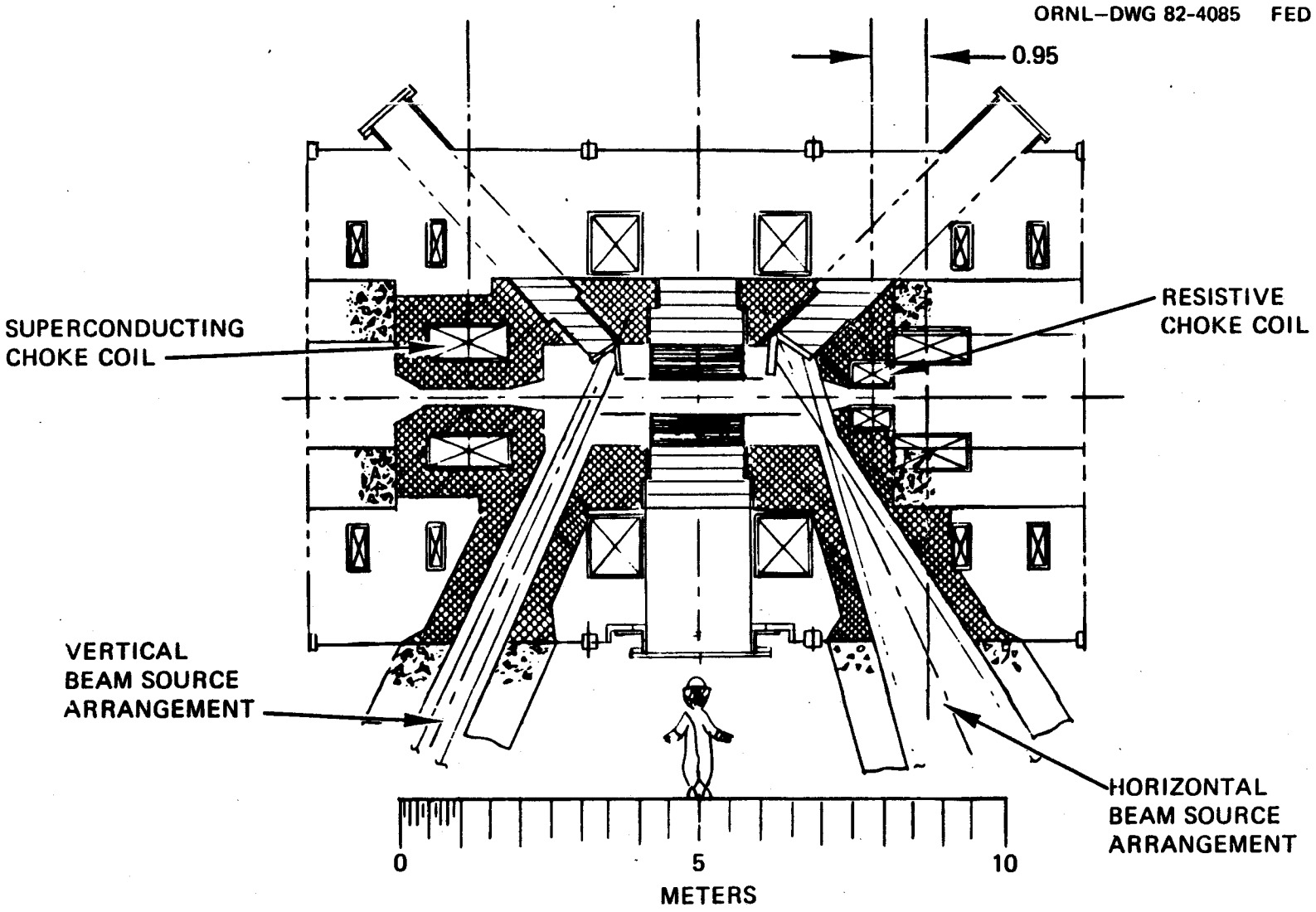

FIGURE 2

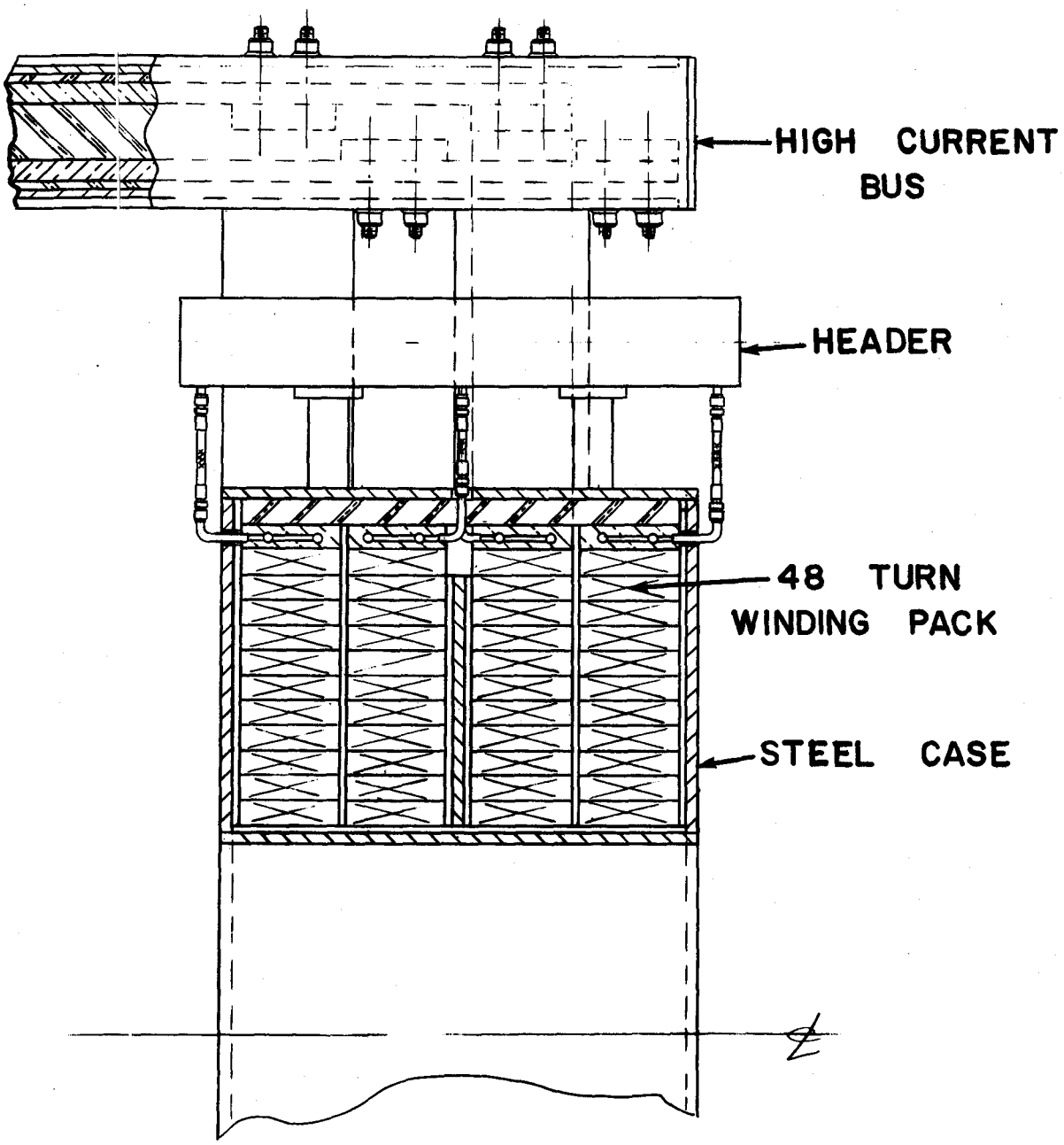

FIGURE 3

NORMAL MAGNET CONCEPT WITH INTERNALLY-COOLED WOUND CONDUCTORS

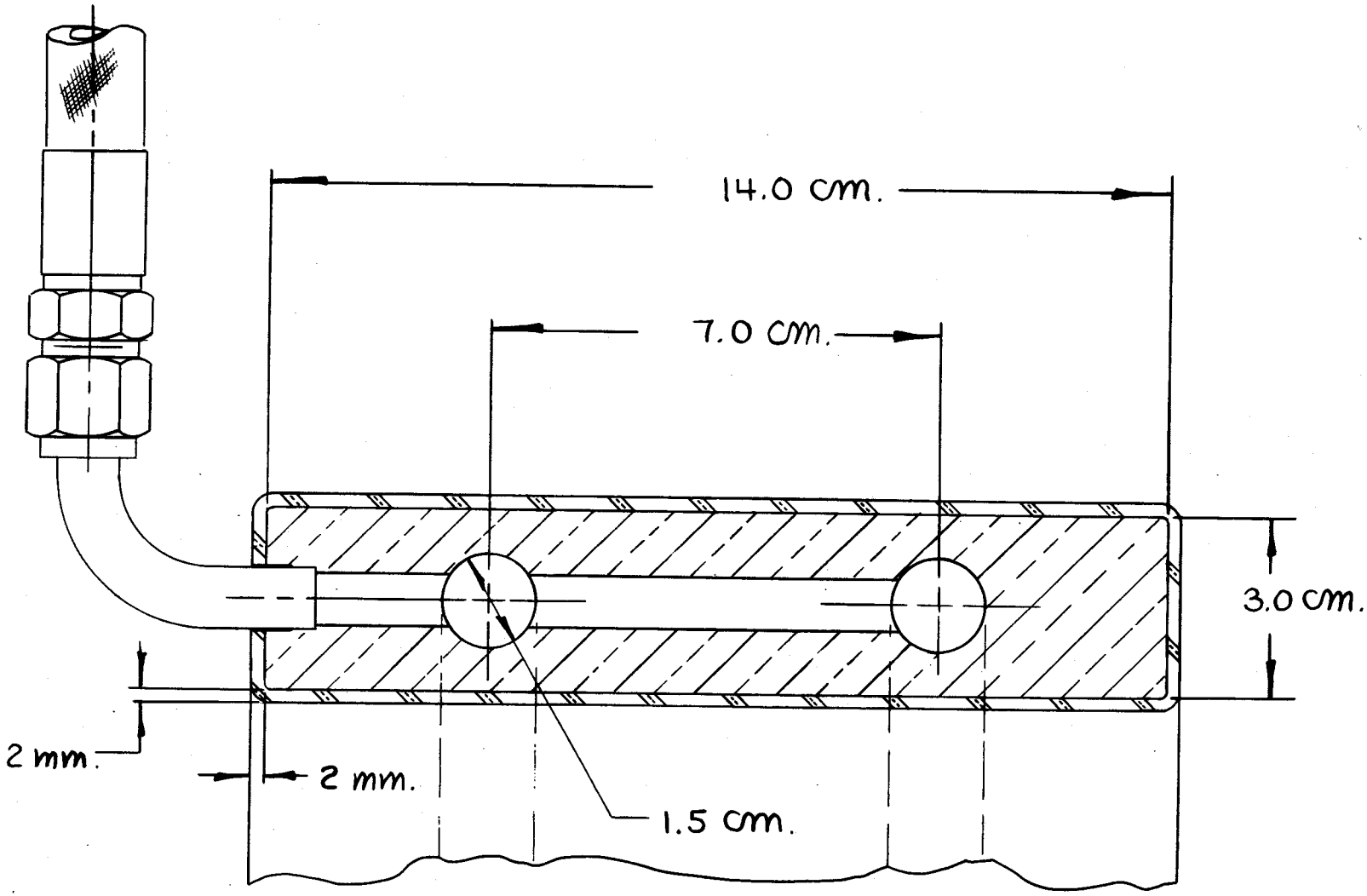

FIGURE 4

CONDUCTOR AND INTERNAL COOLING CONCEPT

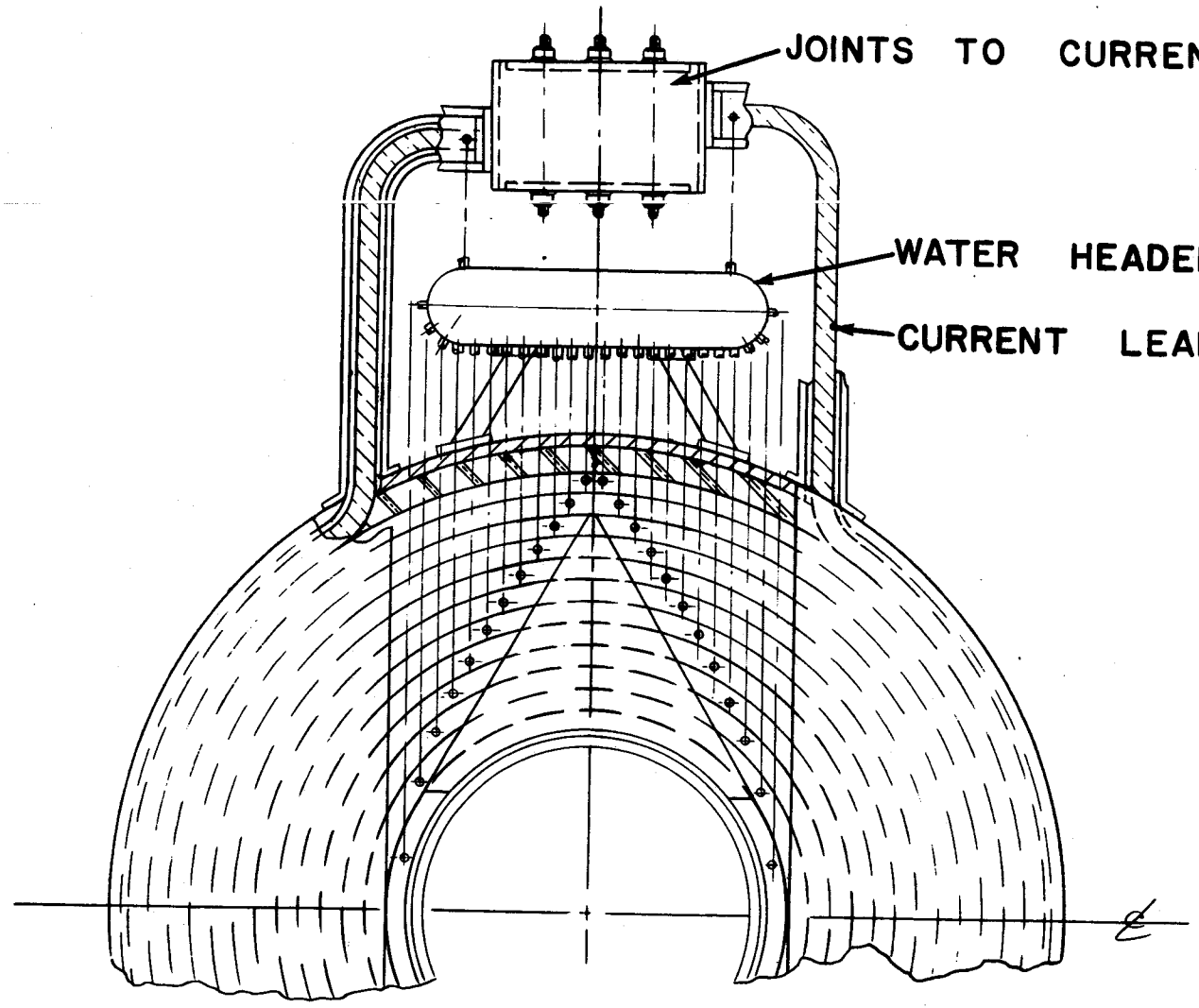

11-28-82

FIGURE 5

AXIAL ELEVATION VIEW OF CROSSECTION OF WOUND NORMAL MAGNET

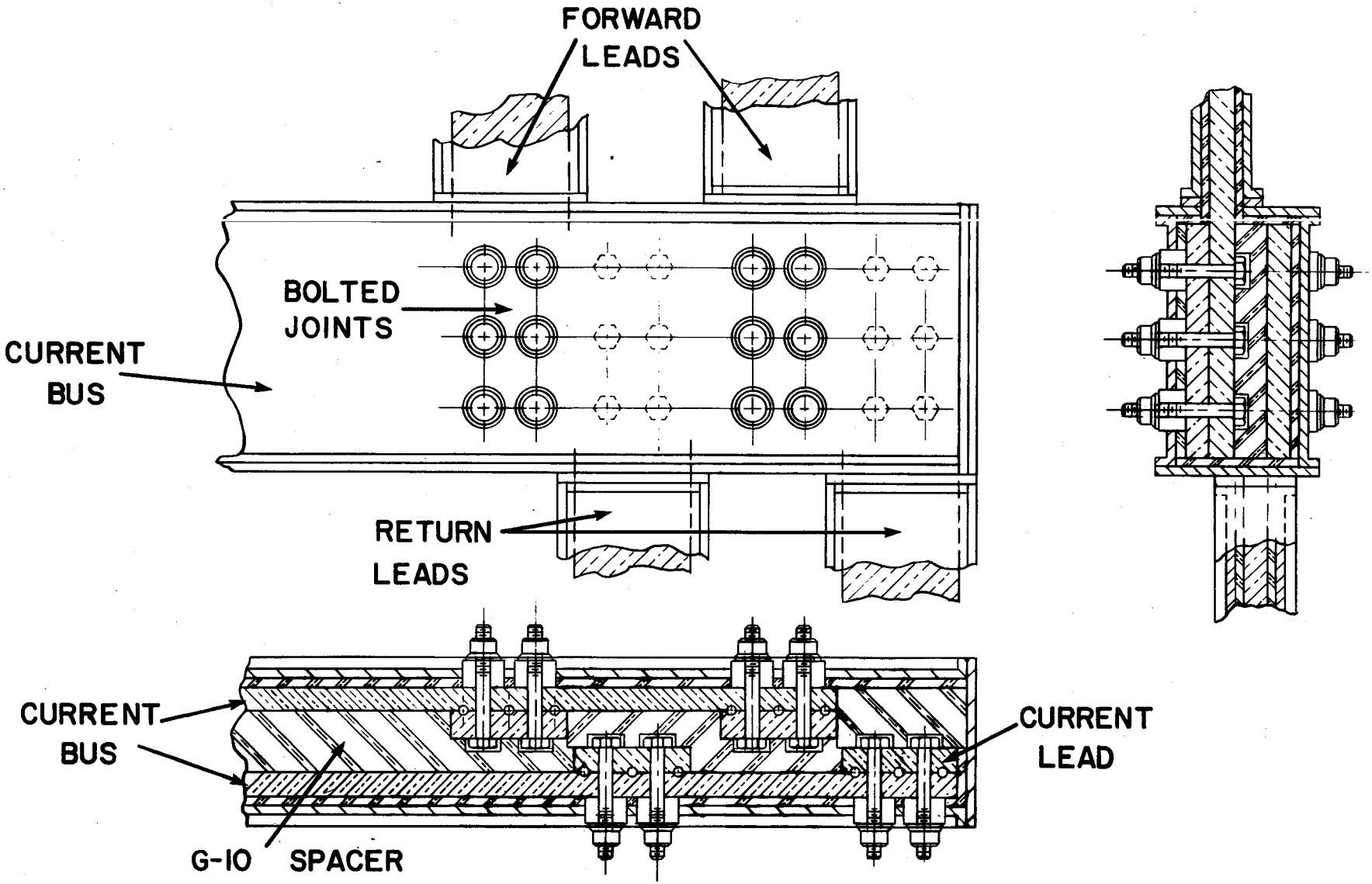

FIGURE 6

LEAD JOINTS TO HIGH CURRENT BUS

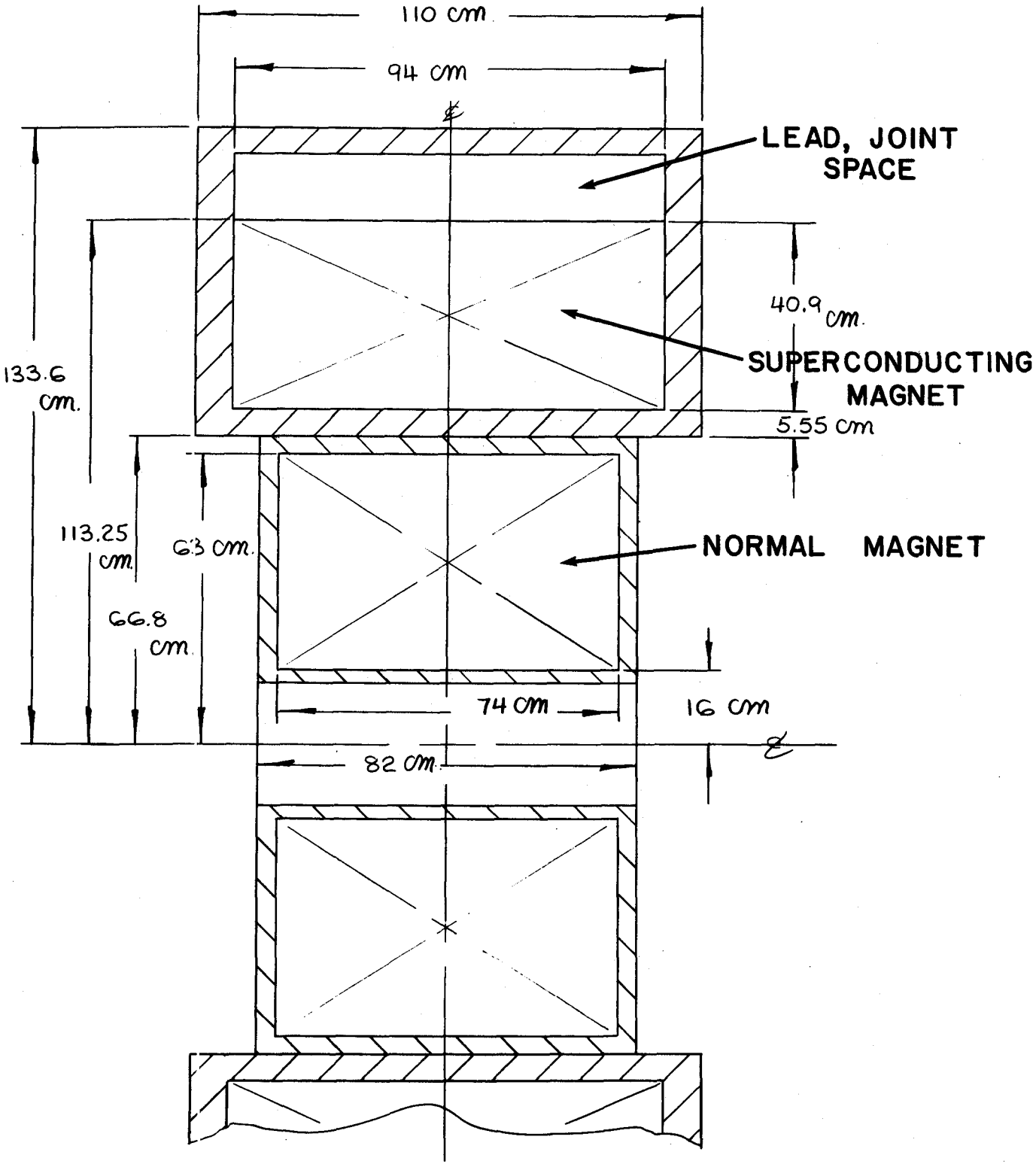

FIGURE 7

HYBRID SUPERCONDUCTING AND NORMAL CHOKE MAGNET SYSTEM

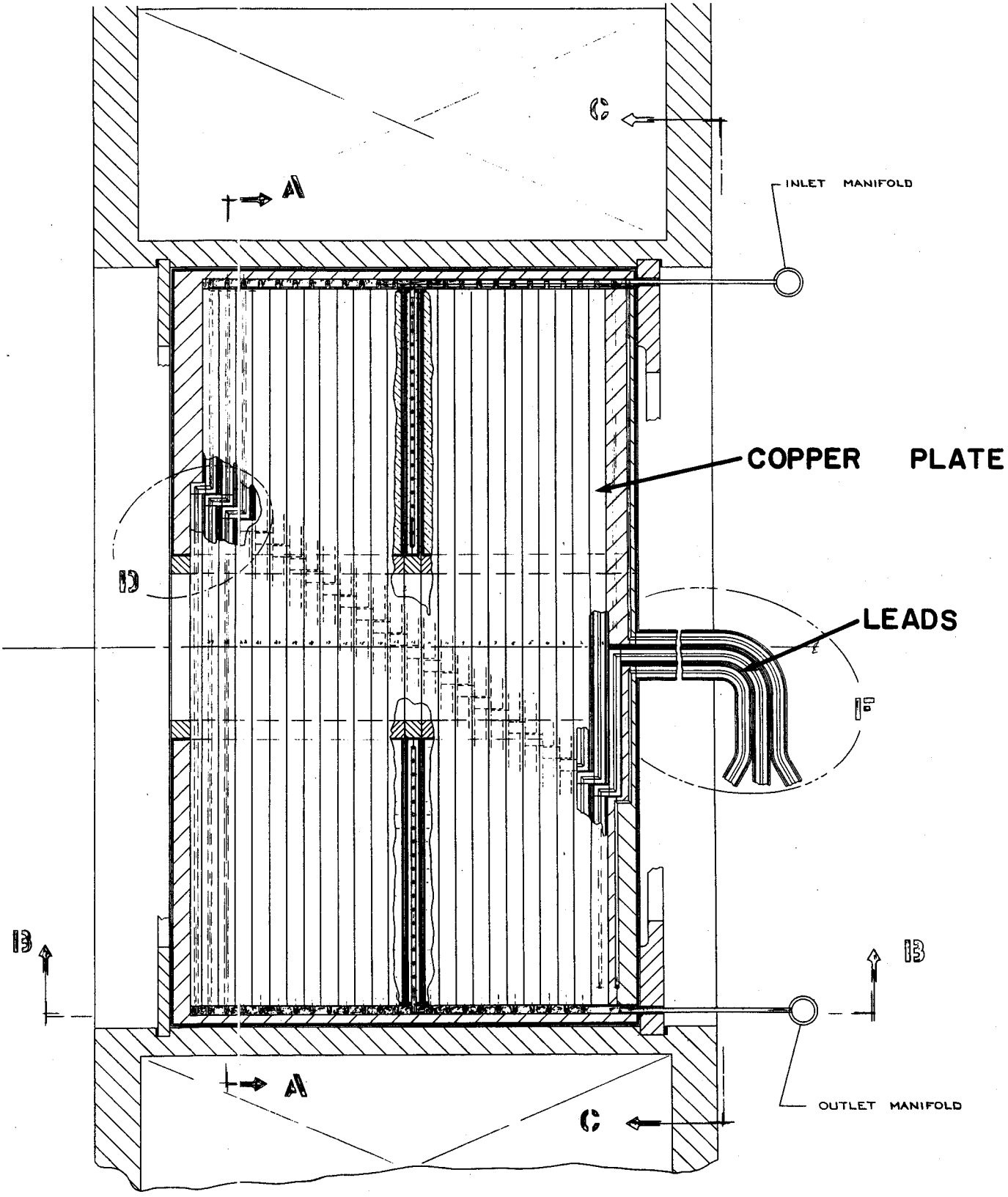

FIGURE 8

BITTER MAGNET CONCEPT IN HYBRID CHOKE SYSTEM

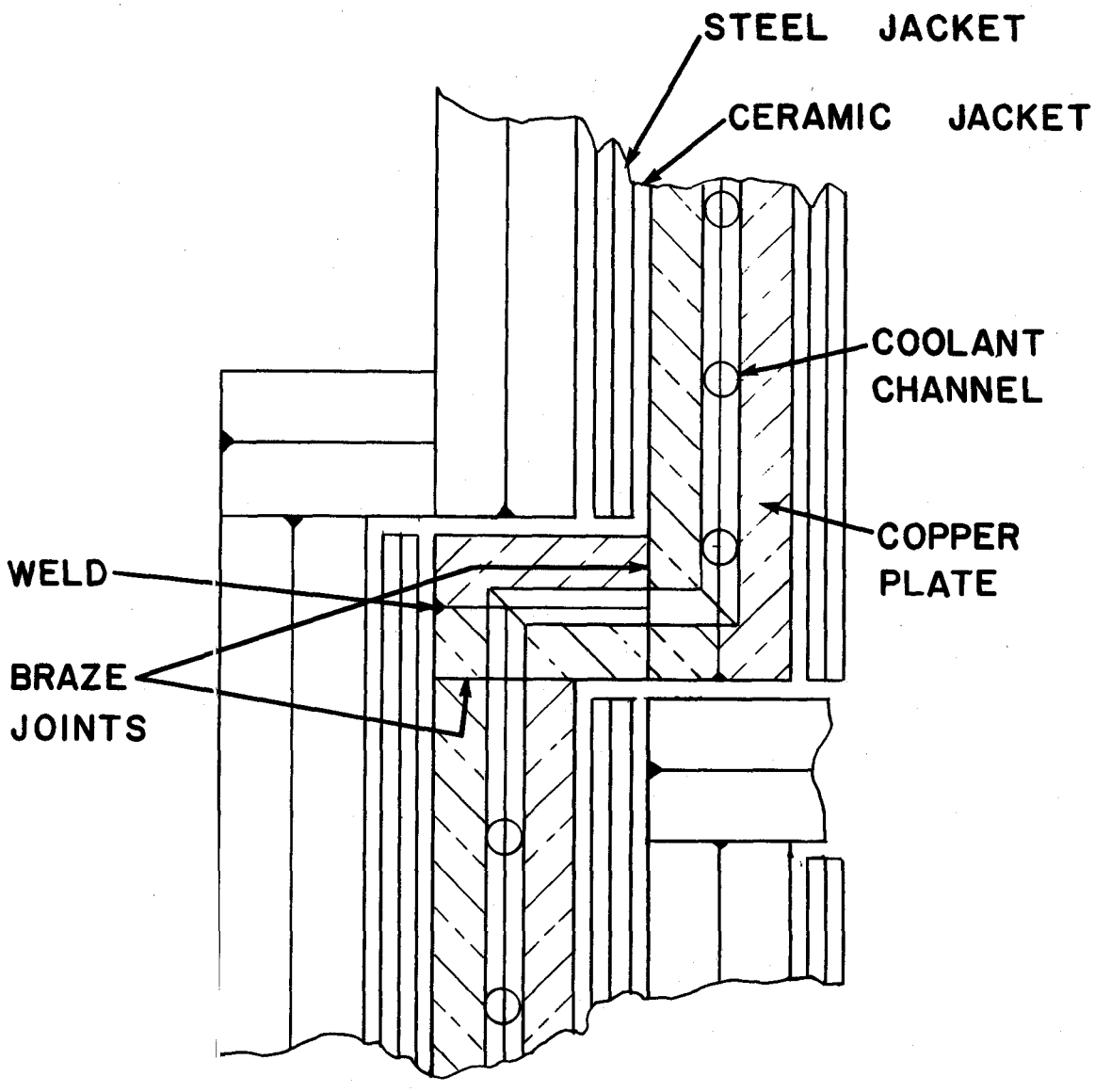

FIGURE 9

INTERNAL JOINT CONCEPT FOR BITTER PLATE MAGNET CONCEPT

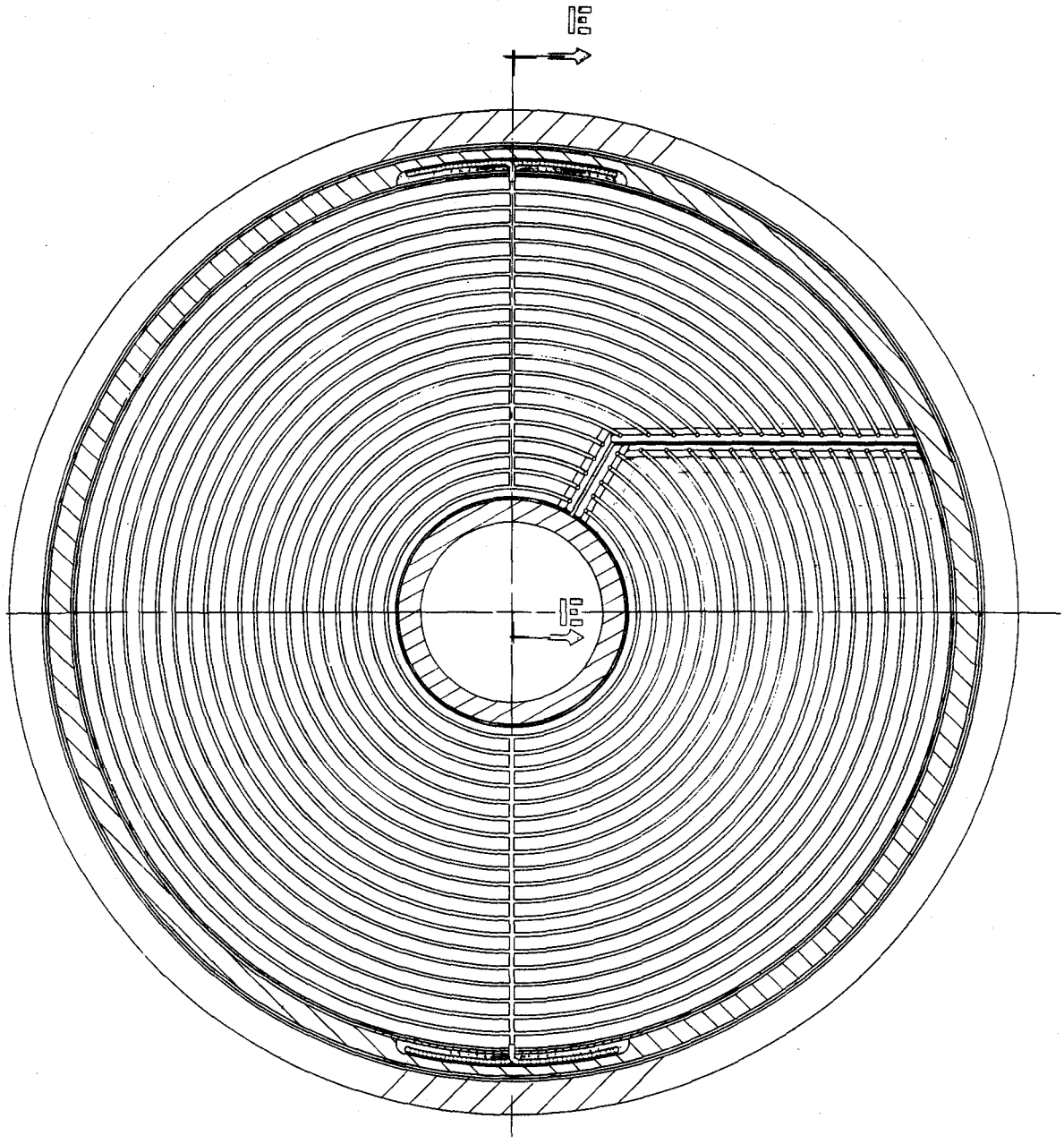

FIGURE 10

BITTER PLATE COOLING CHANNEL CONCEPT

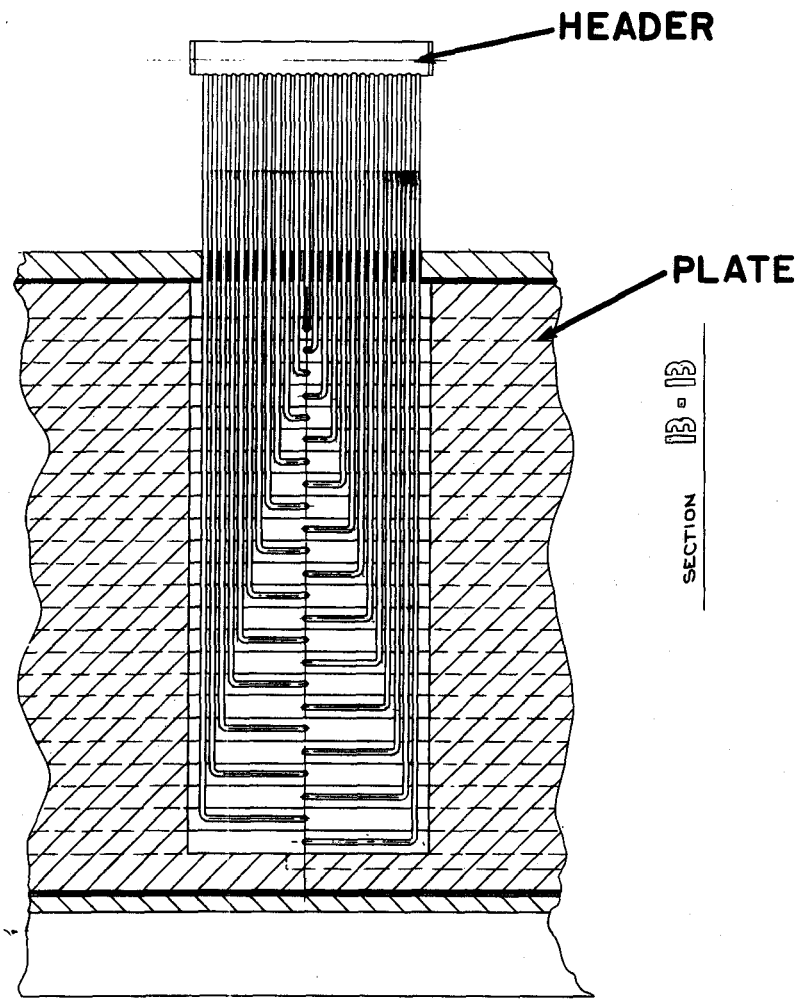

FIGURE 11

INTERNAL HEADER CONNECTIONS TO BITTER PLATE COOLING CHANNELS

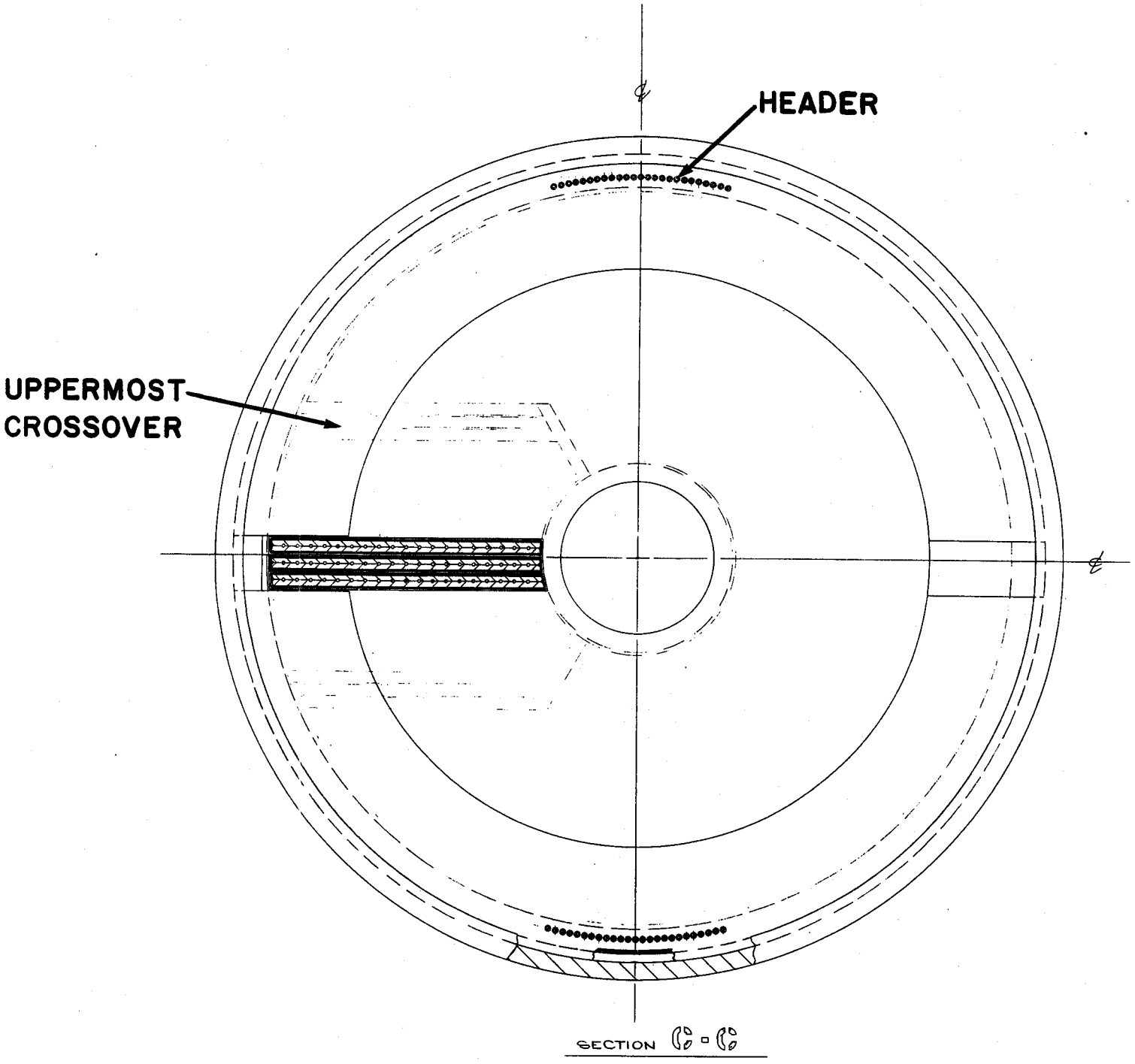

FIGURE 12

INTERNAL CROSSOVERS BETWEEN
BITTER MAGNET PLATES

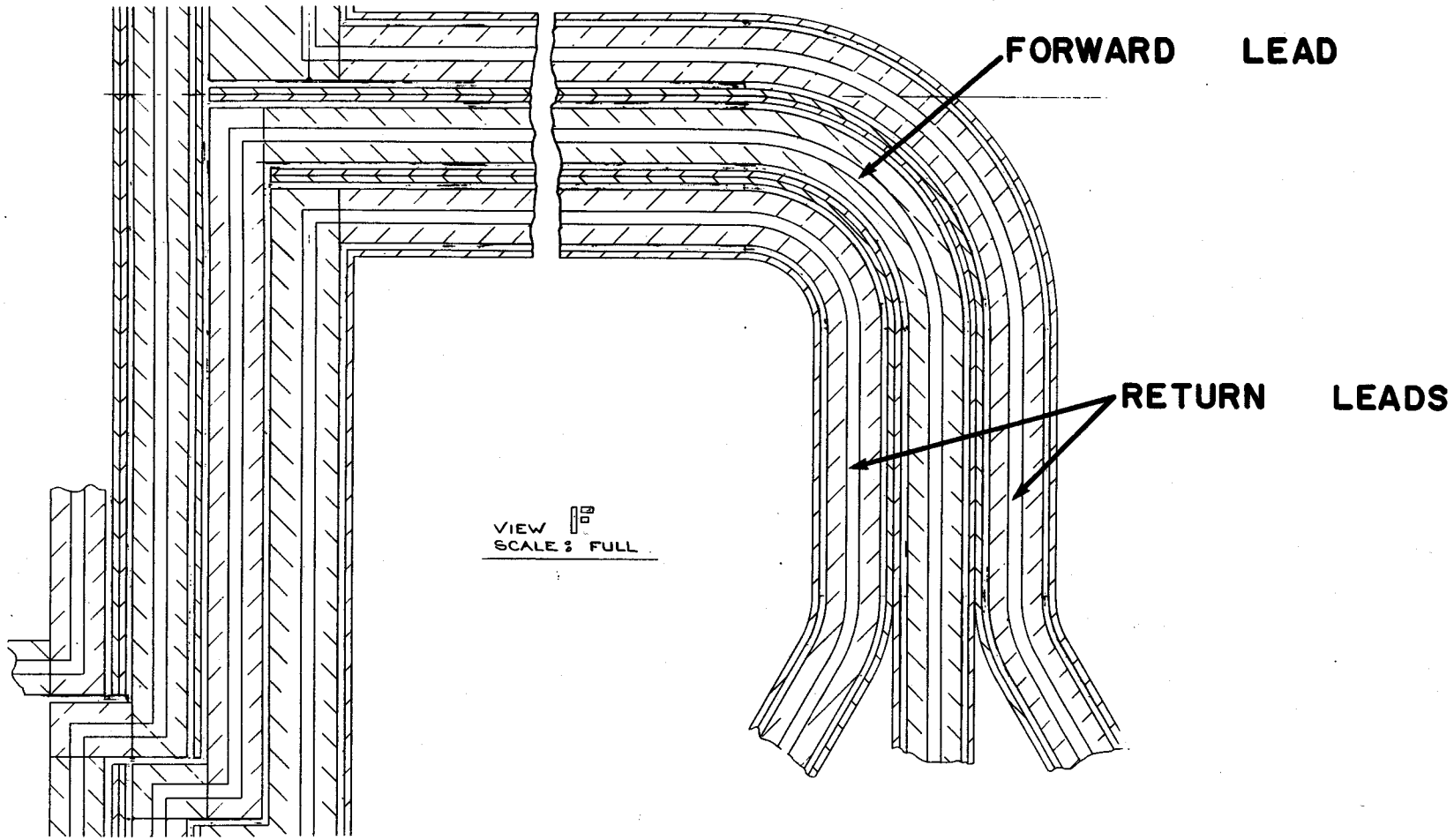

FIGURE 13

LEADS WITH RETAINED INSULATION,
BITTER PLATE MAGNET CONCEPT

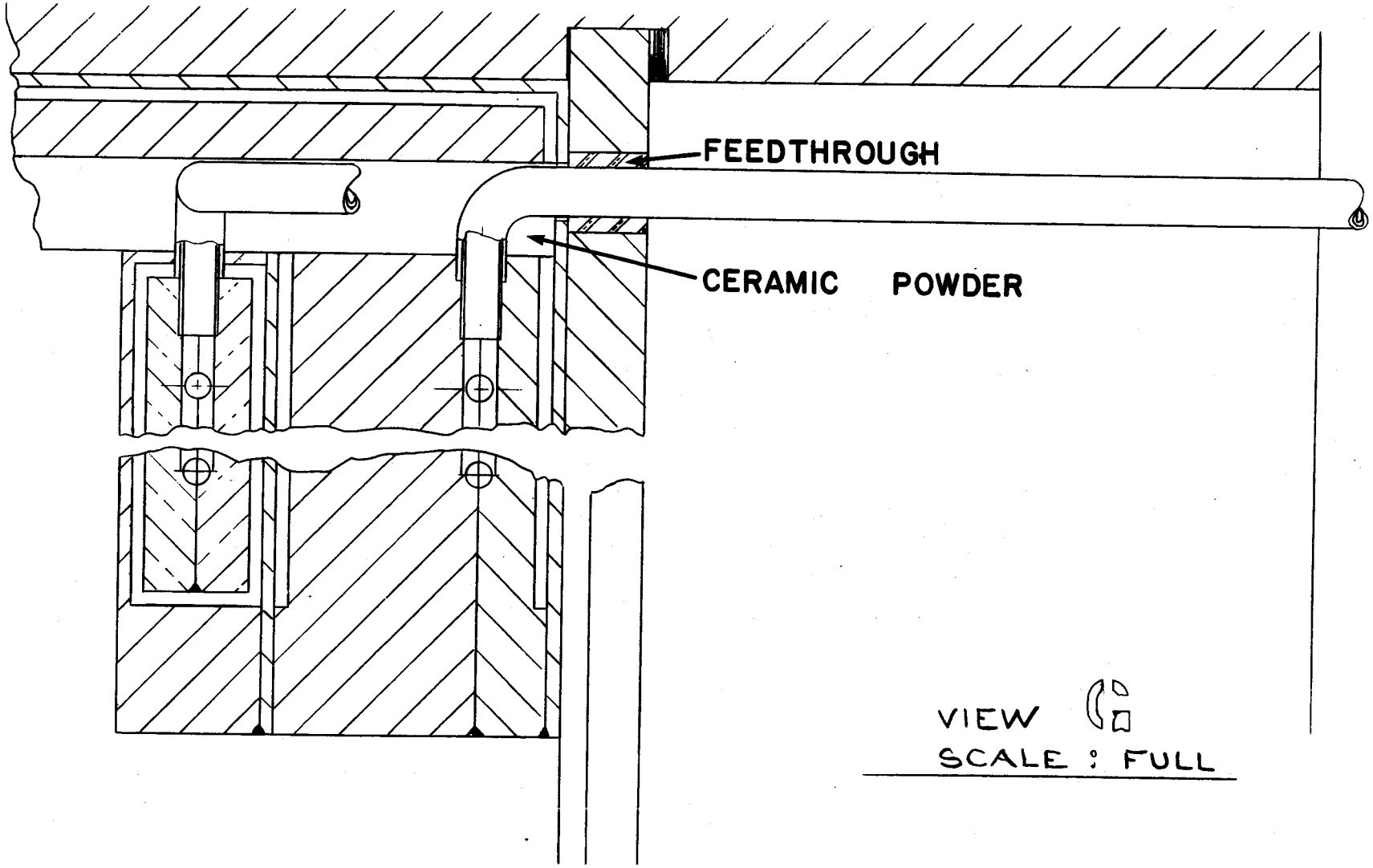

FIGURE 14

COOLANT PENETRATION TO INTERNAL HEADER
BITTER PLATE MAGNET CONCEPT

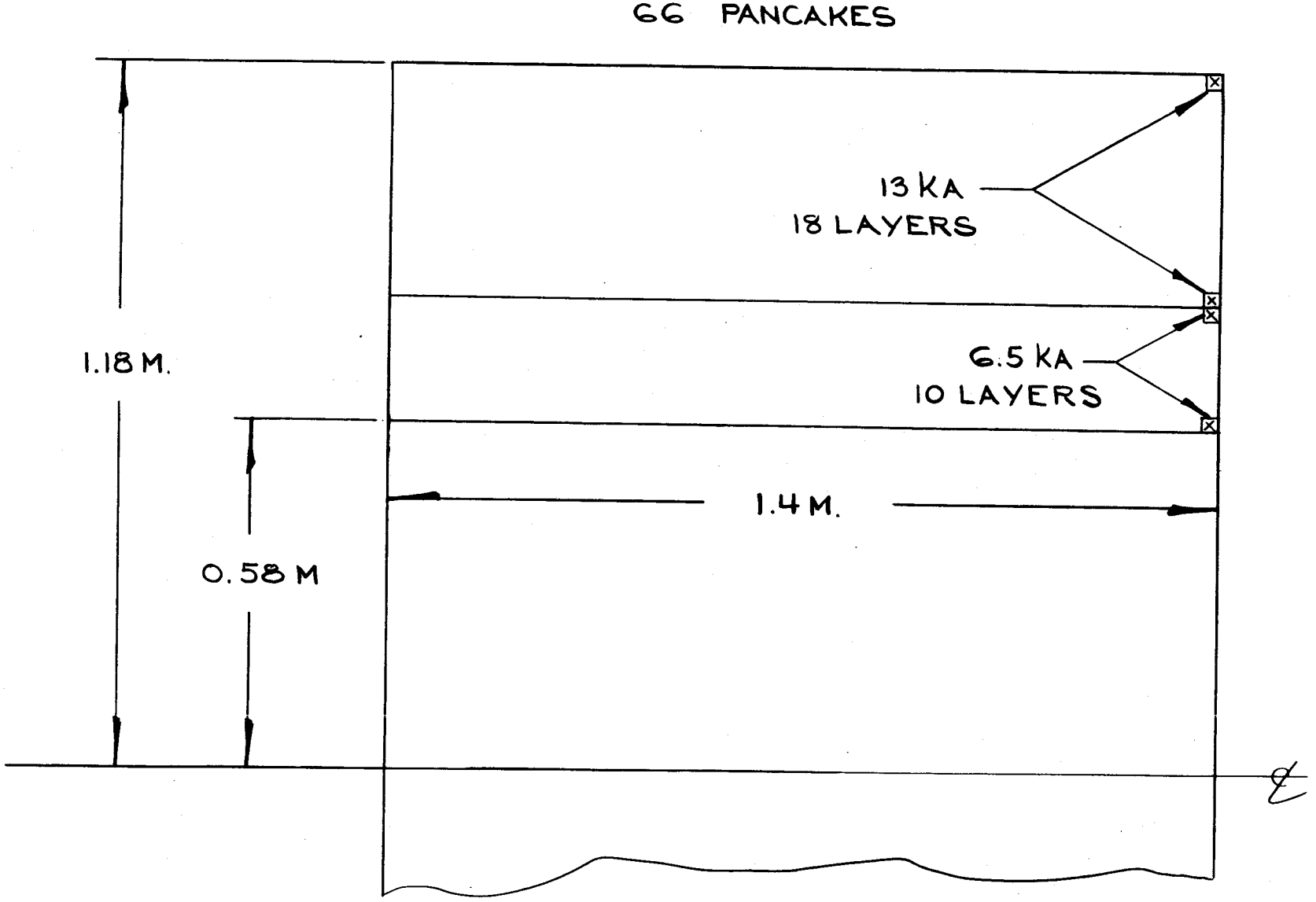

FIGURE 15

GRATED SUPERCONDING CHOKE COIL SYSTEM CONCEPT

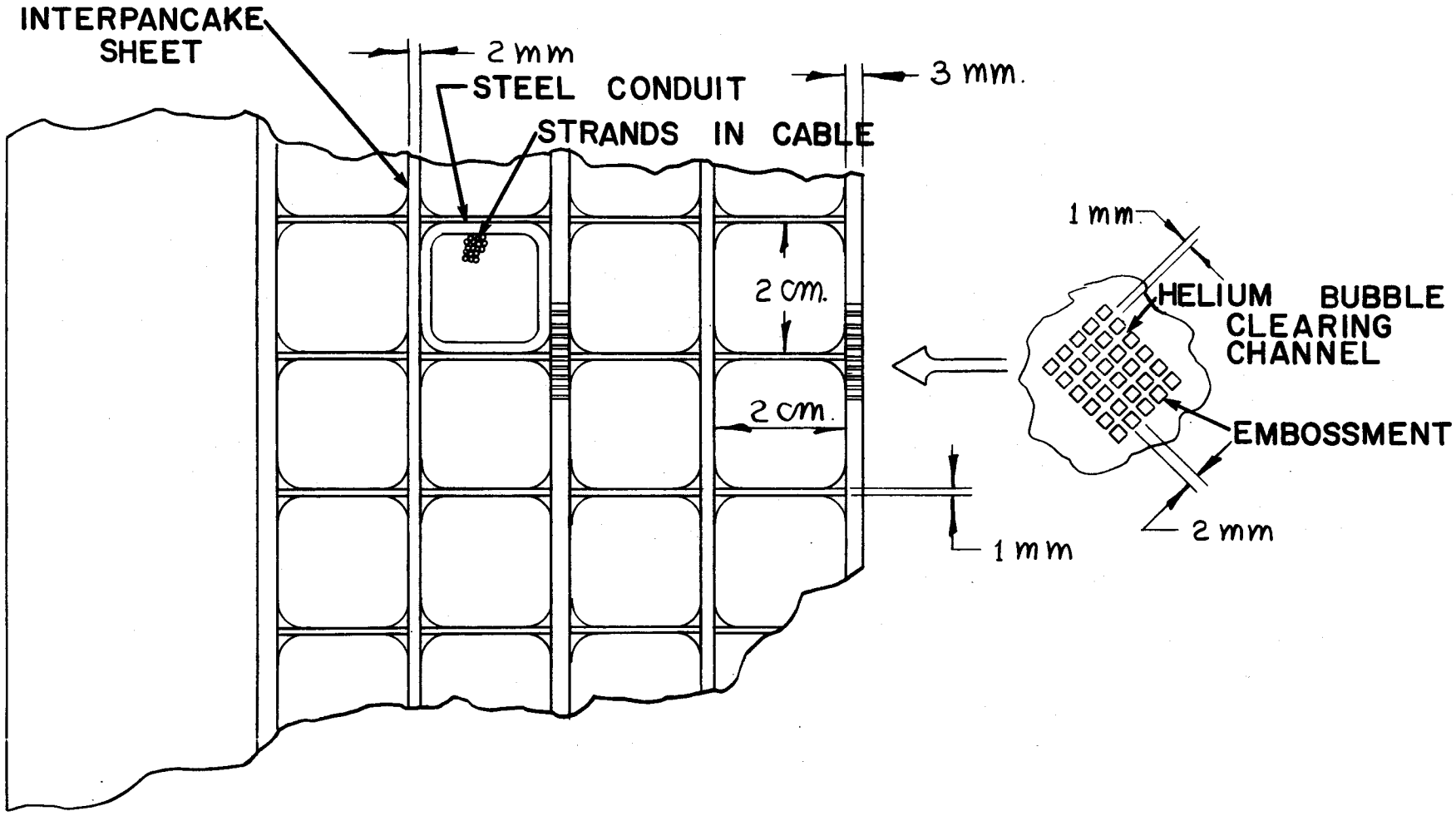

FIGURE 16

INTERNALLY CABLED, EXTERNALLY POOL COOLED
WINDING PACK CONCEPT

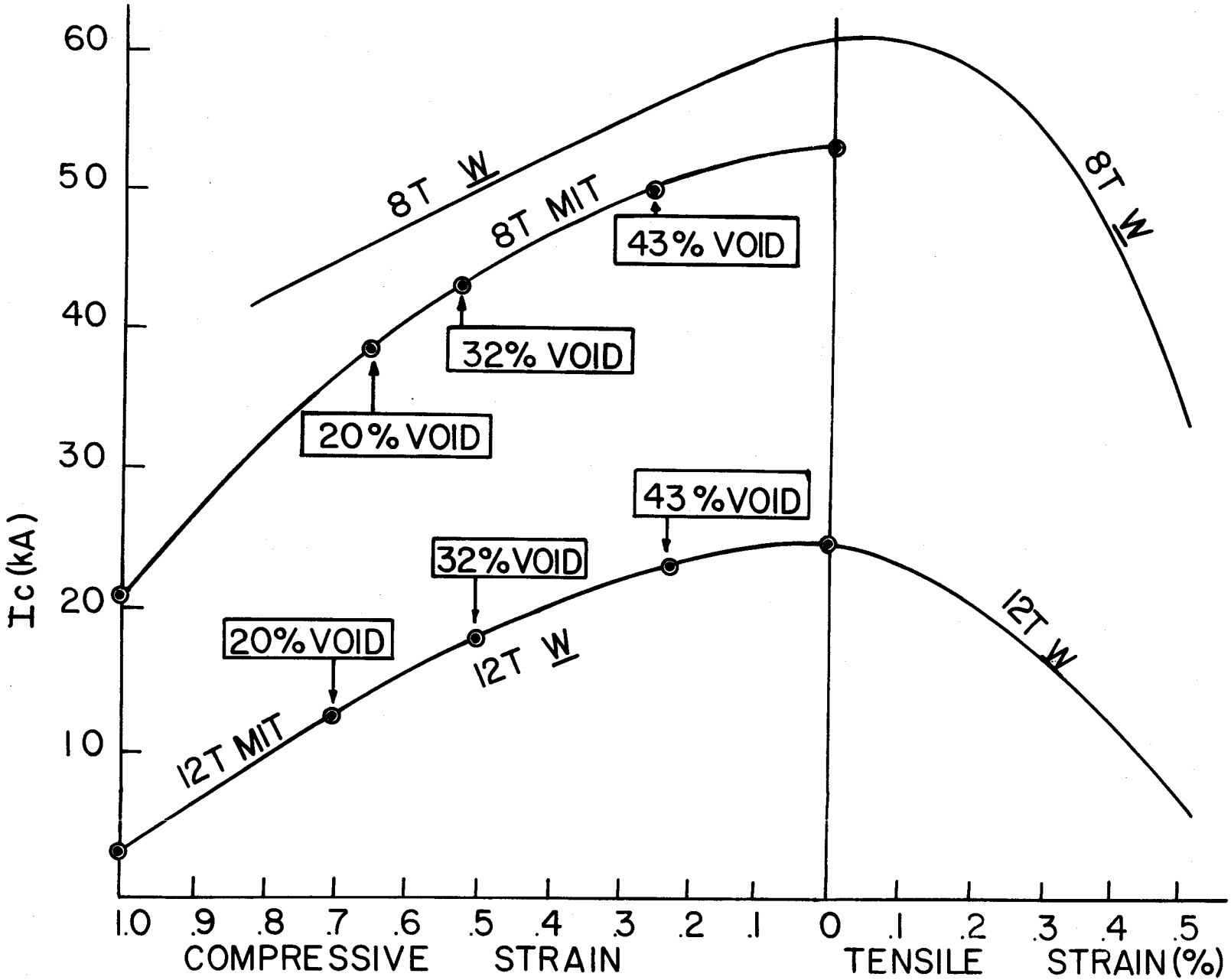

FIGURE 17

LCP(W) Conductor Critical Current Ic vs. Strain at 12 & 8T

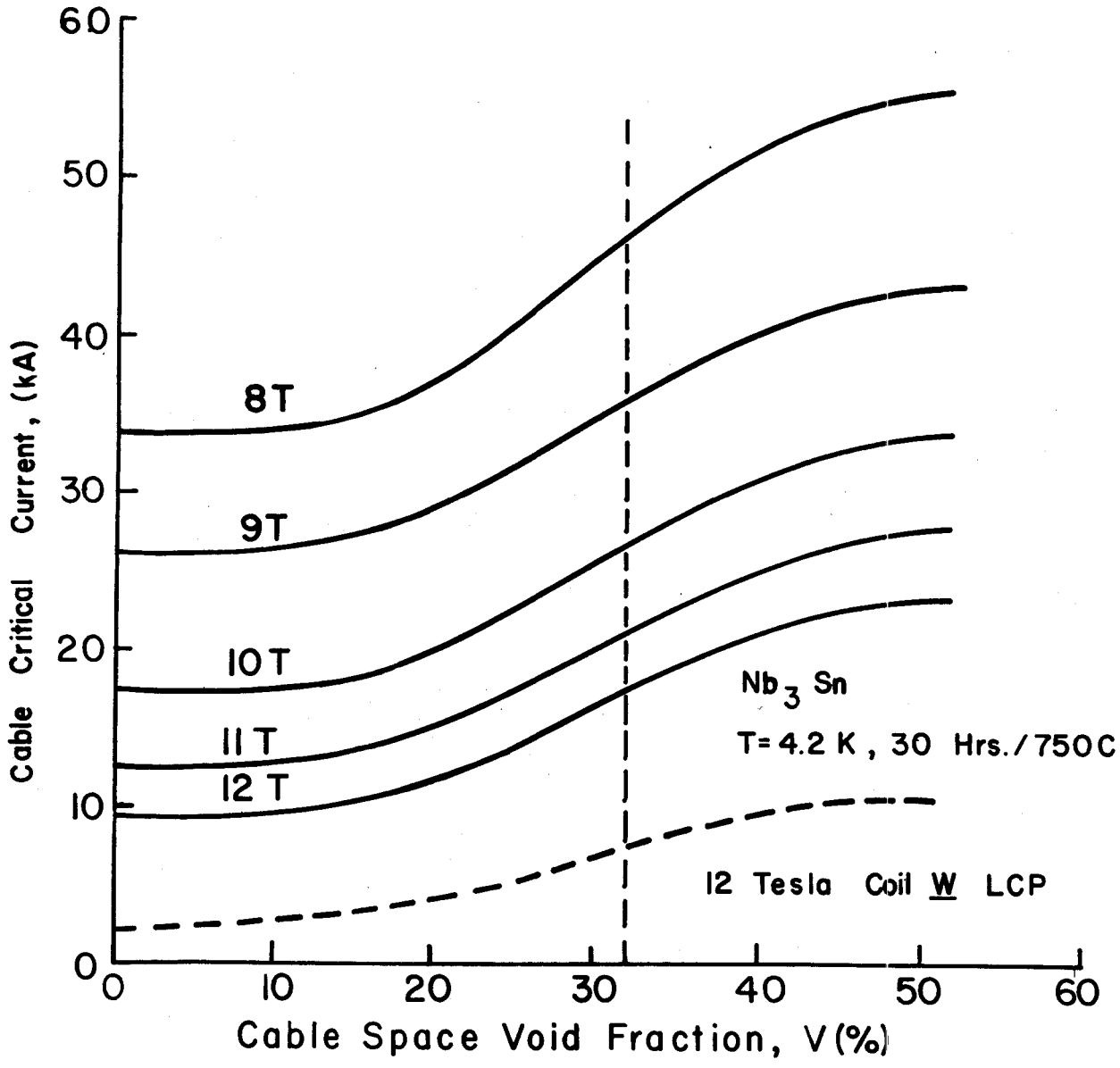

FIGURE 18

Predicted Critical Current as a Function of Cable Space Void Fraction. The cable consists of 486 strands of Airco 0.7 mm Diameter Nb_3Sn wire. Void fraction equals the space available to helium. The data is from conductors reacted at 750°C and tested at 4.2 K. Both the Westinghouse LCP and

FIGURE 19

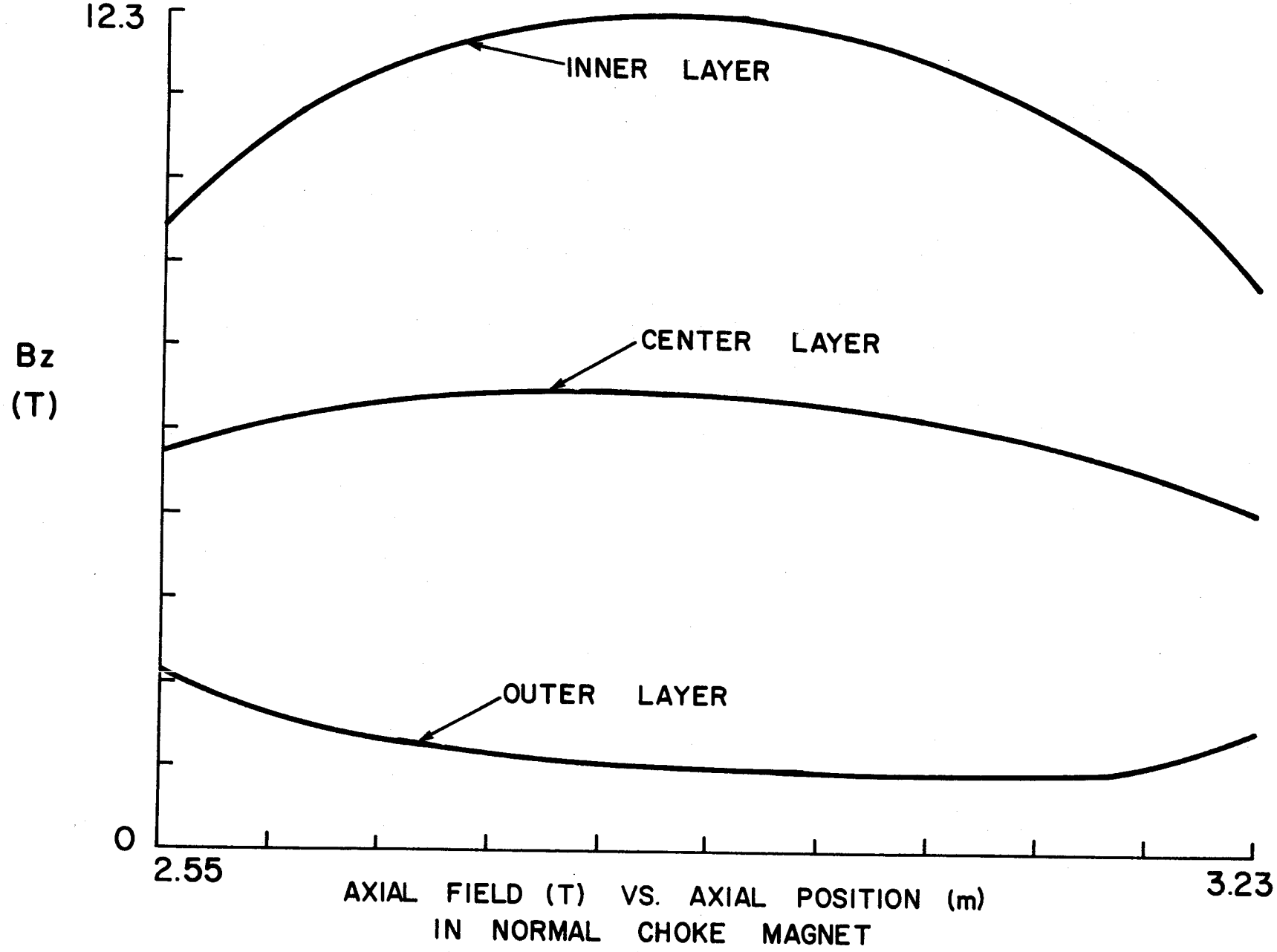
12.3
INNER LAYER
CENTER LAYER
OUTER LAYER
Bz
(T)
0
2.55
3.23
AXIAL FIELD (T) VS. AXIAL POSITION (m)
IN NORMAL CHOKE MAGNET

FIGURE 20

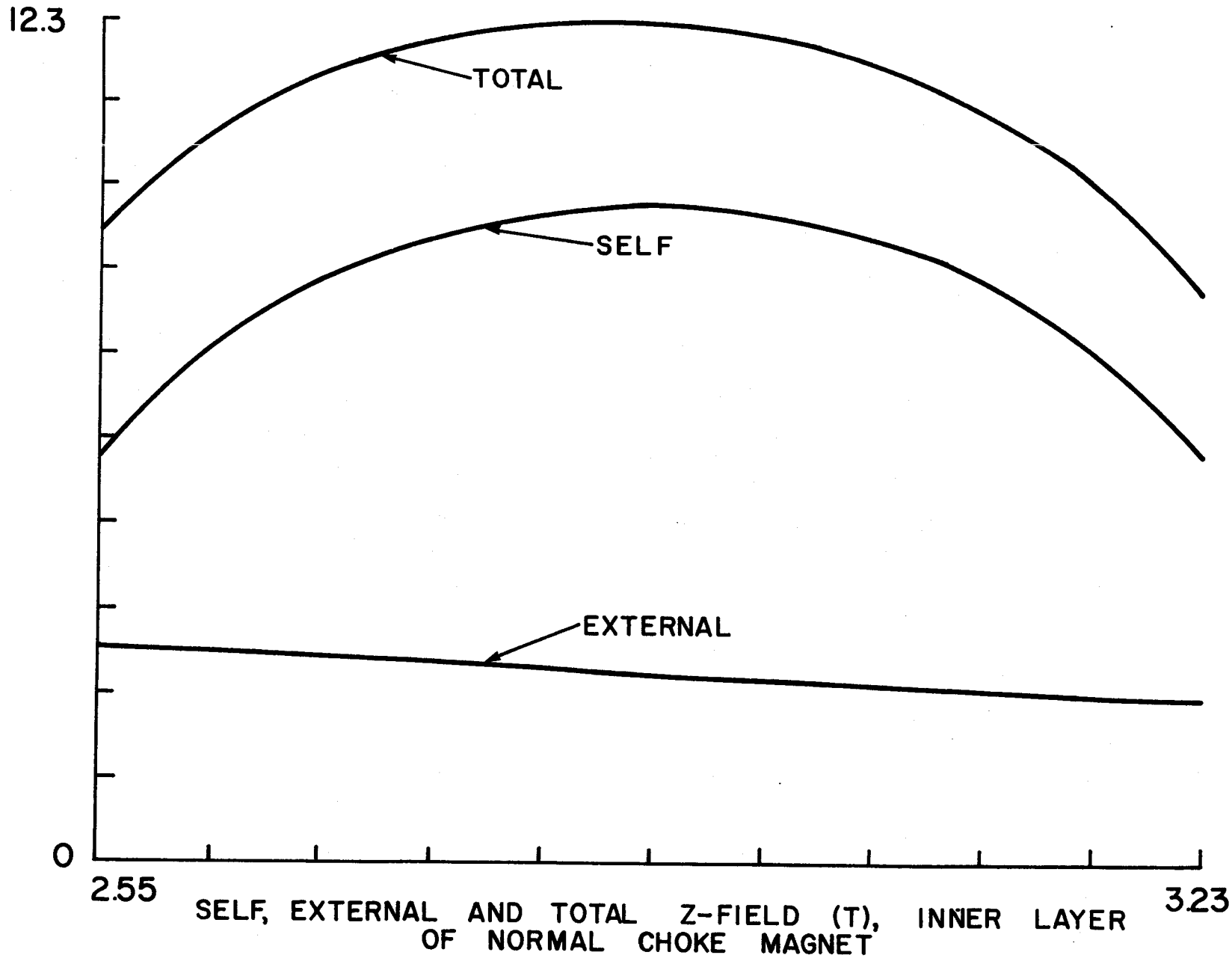

SELF, EXTERNAL AND TOTAL Z-FIELD (T), INNER LAYER OF NORMAL CHOKE MAGNET

FIGURE 21

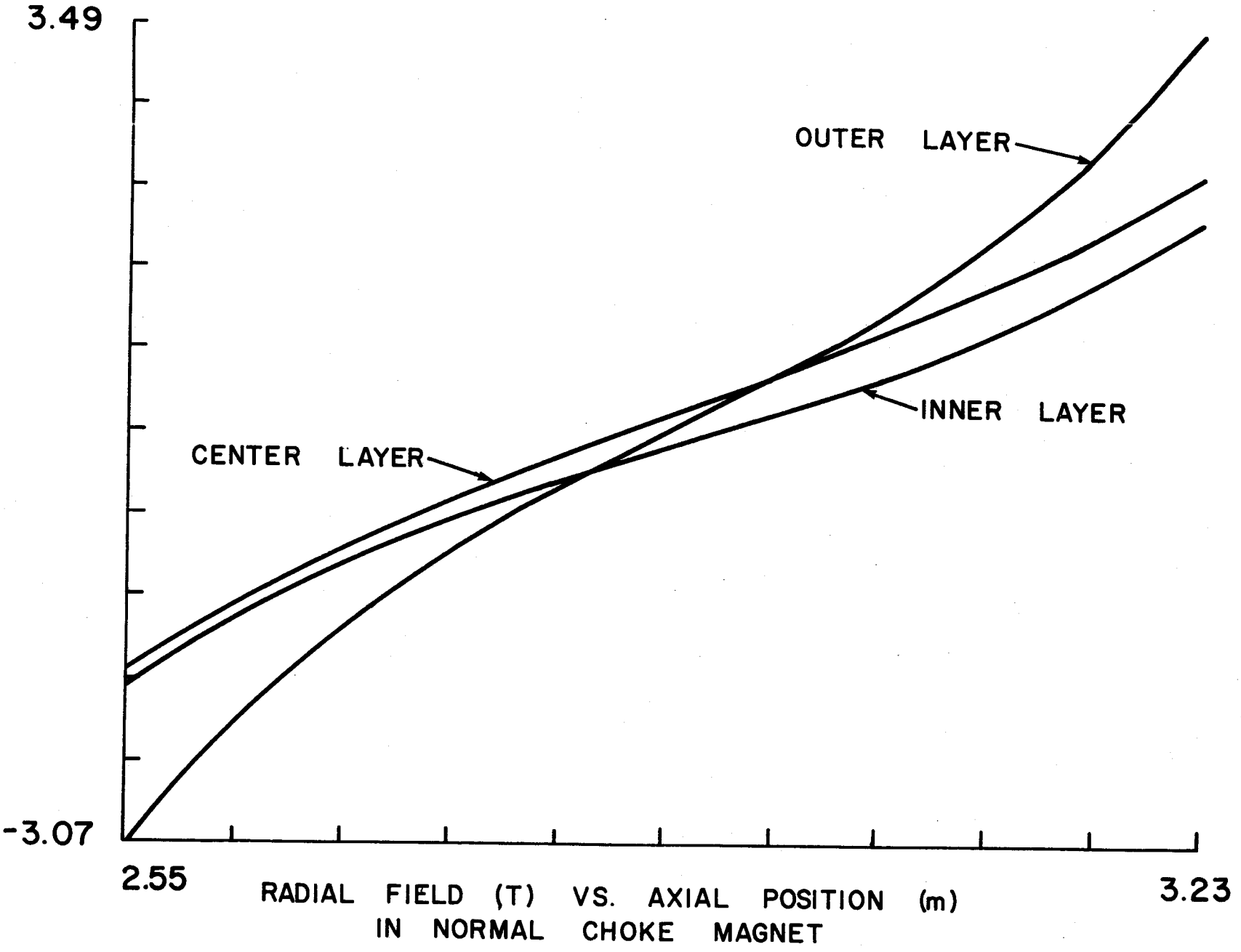
3.49
OUTER LAYER
INNER LAYER
CENTER LAYER
-3.07
2.55
3.23
RADIAL FIELD (T) VS. AXIAL POSITION (m)
IN NORMAL CHOKE MAGNET

FIGURE 22

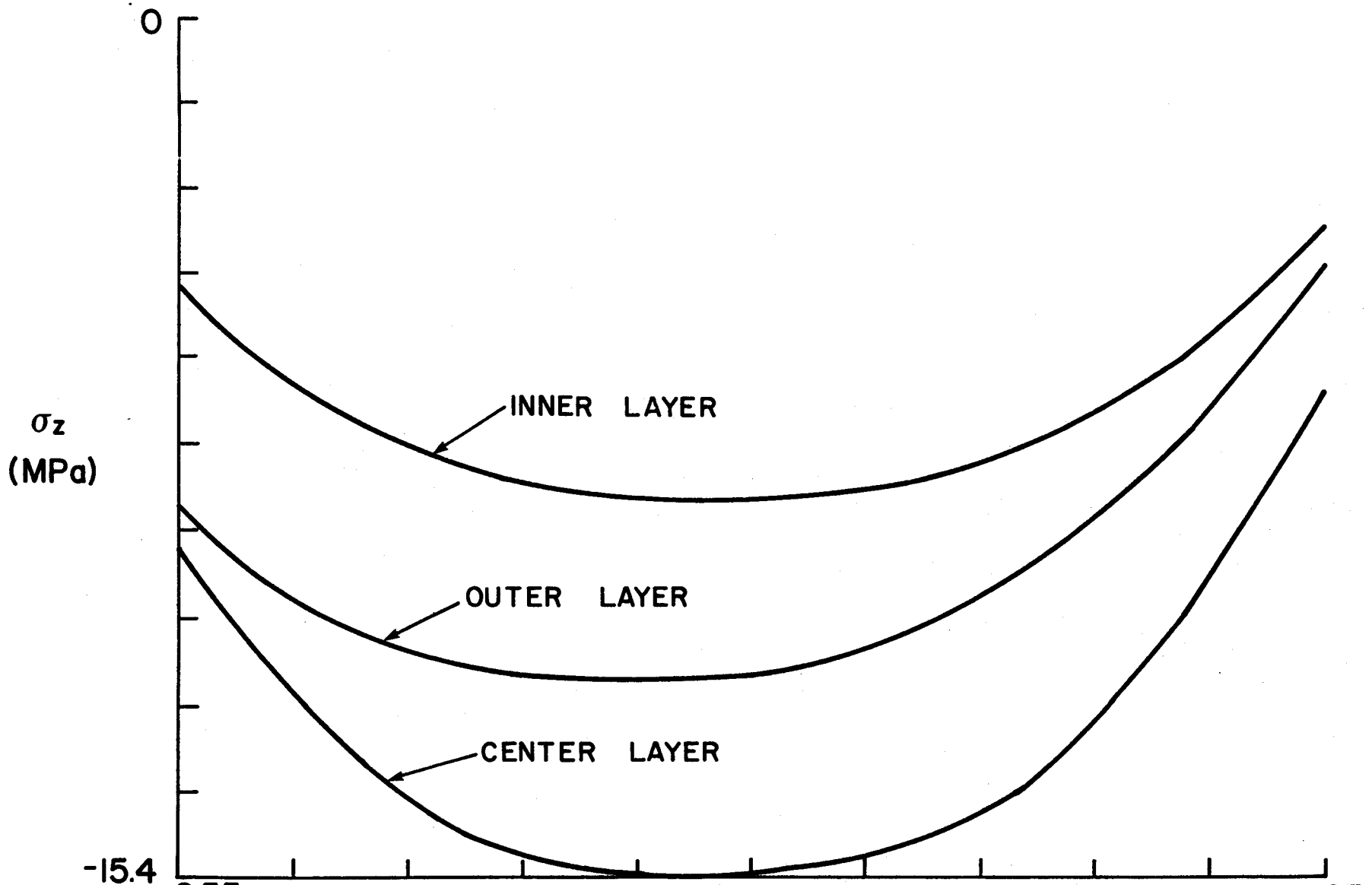

AXIAL STRESSES (MPa) IN NORMAL CHOKE COIL, ASSUMED TO BE SELF-SUPPORTING, VS. AXIAL POSITION

FIGURE 23

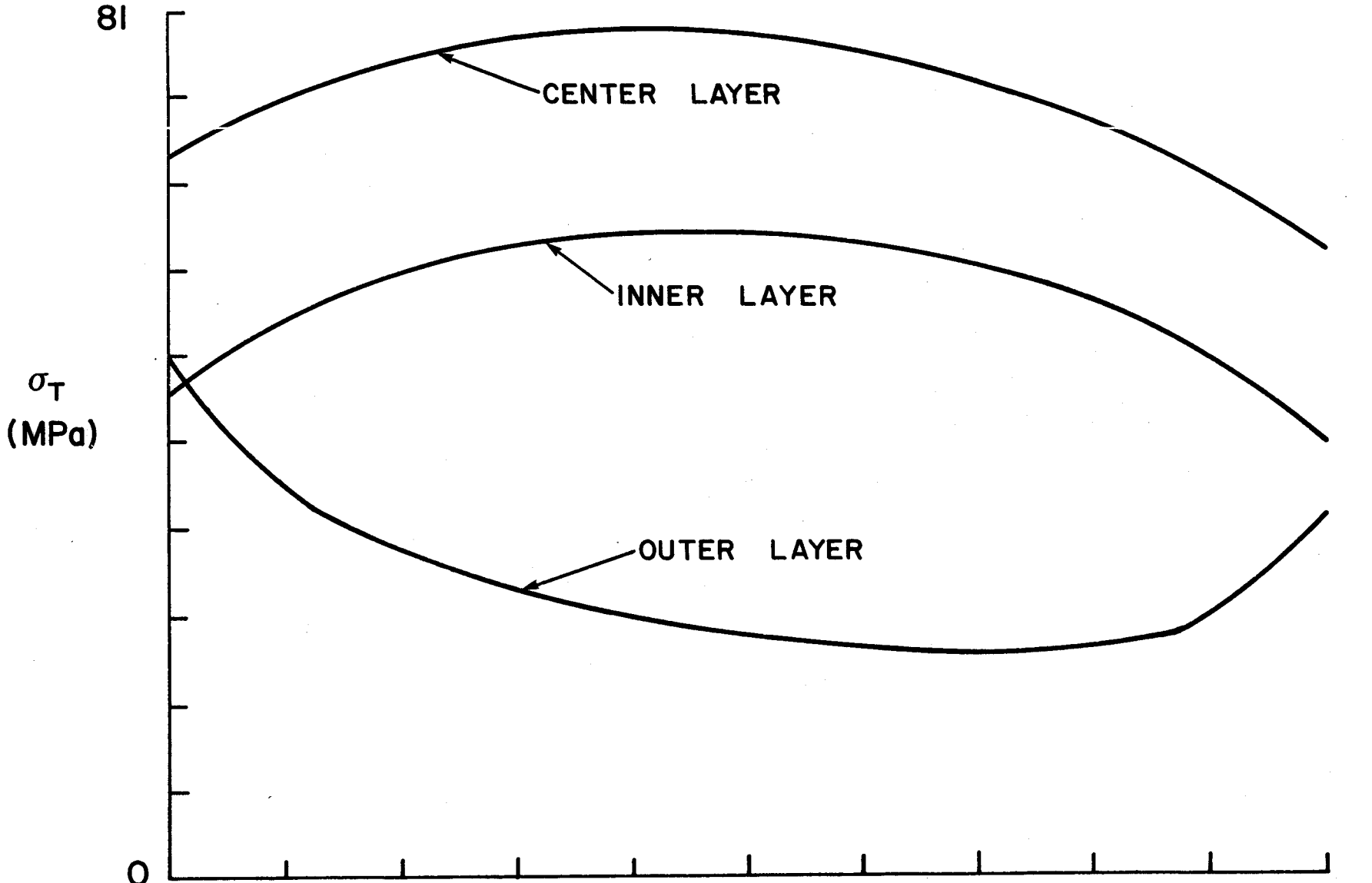

HOOP STRESS (MPa) IN NORMAL MAGNET CONDUCTORS, ASSUMED TO BE SELF-SUPPORTING, VS. AXIAL POSITION (m)

FIGURE 24

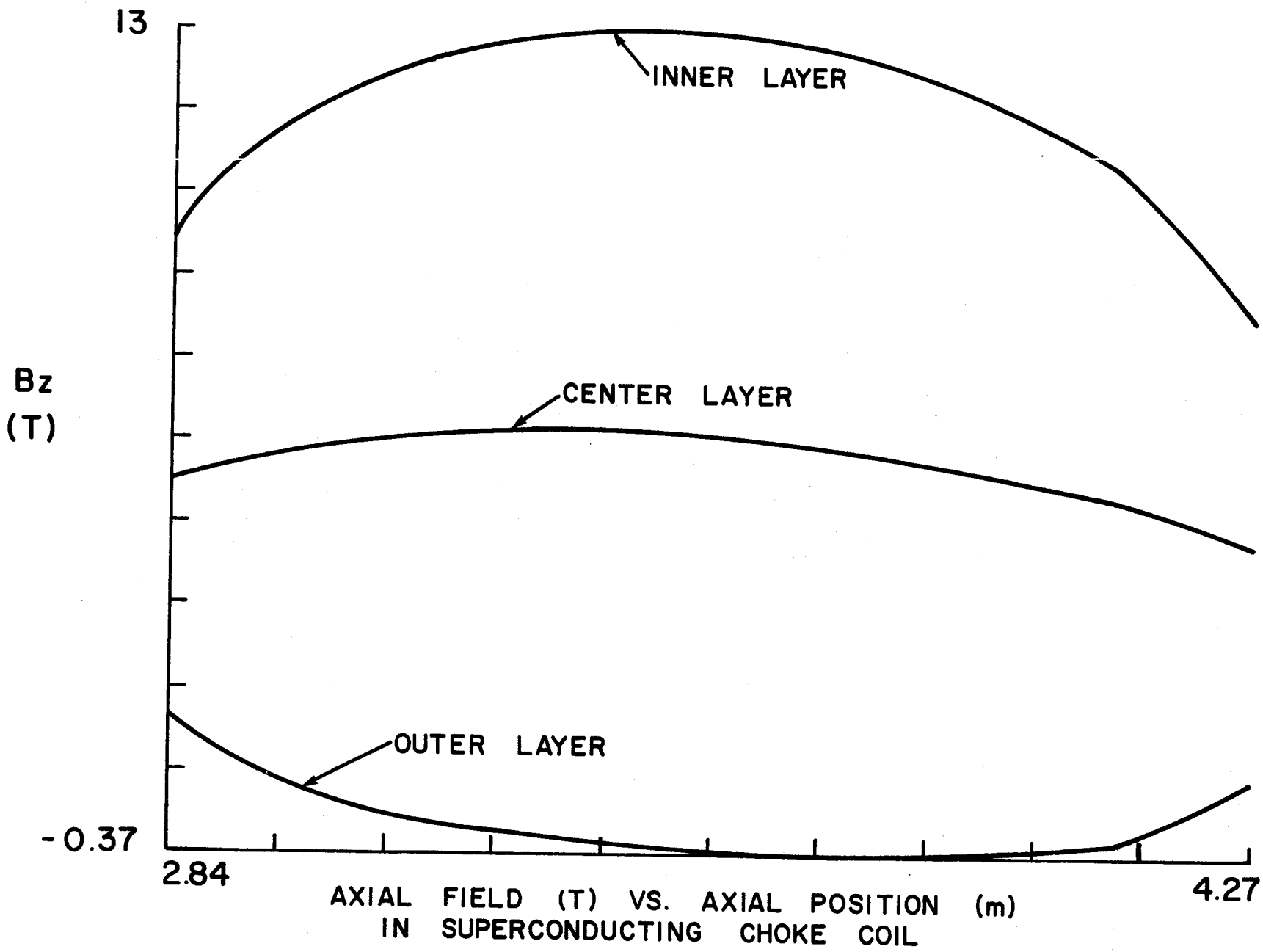

AXIAL FIELD (T) VS. AXIAL POSITION (m)
IN SUPERCONDUCTING CHOKE COIL

FIGURE 25

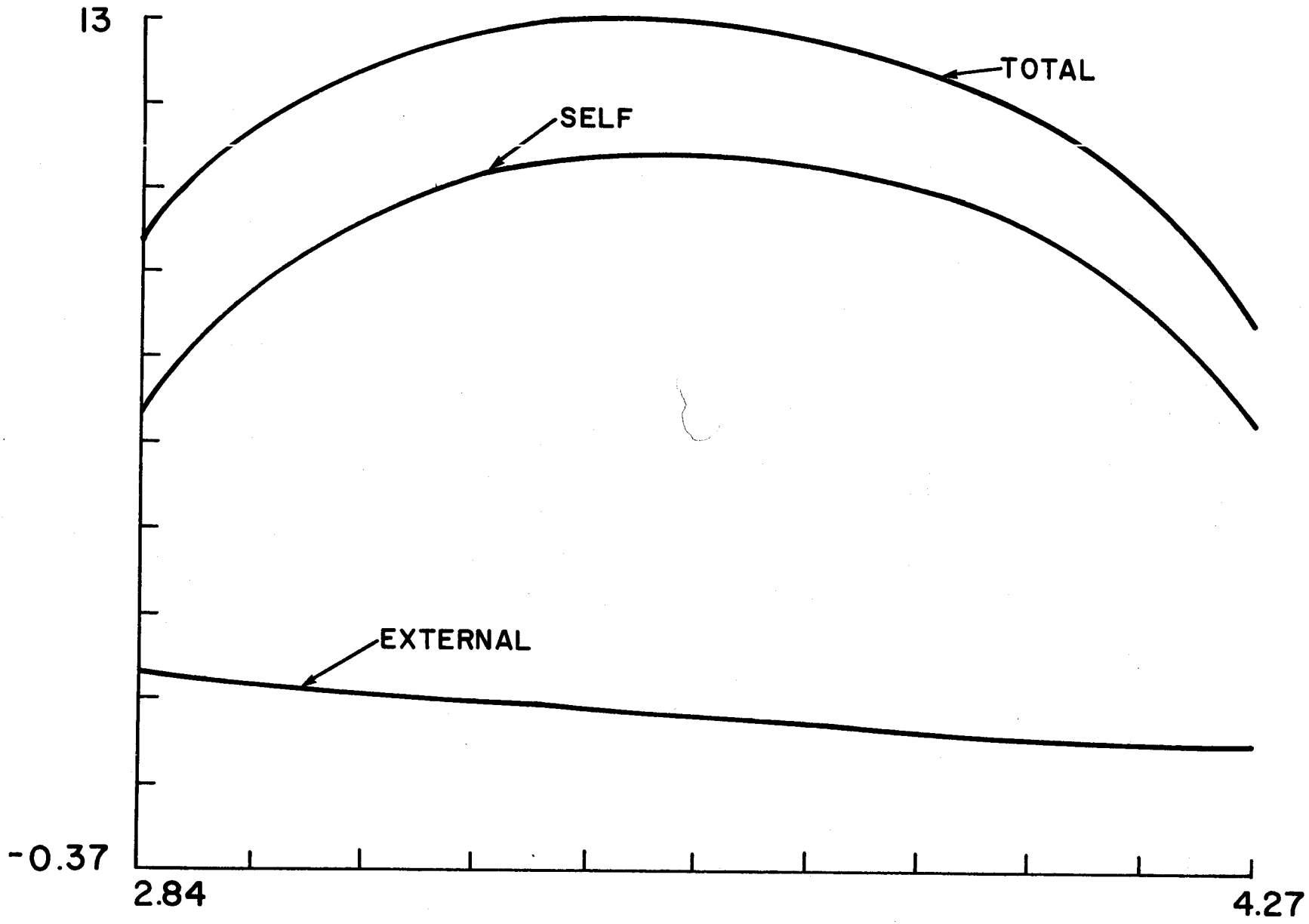

SELF, EXTERNAL AND TOTAL Z-FIELD (T), INNER LAYER OF SUPERCONDUCTING CHOKE (m)

FIGURE 26

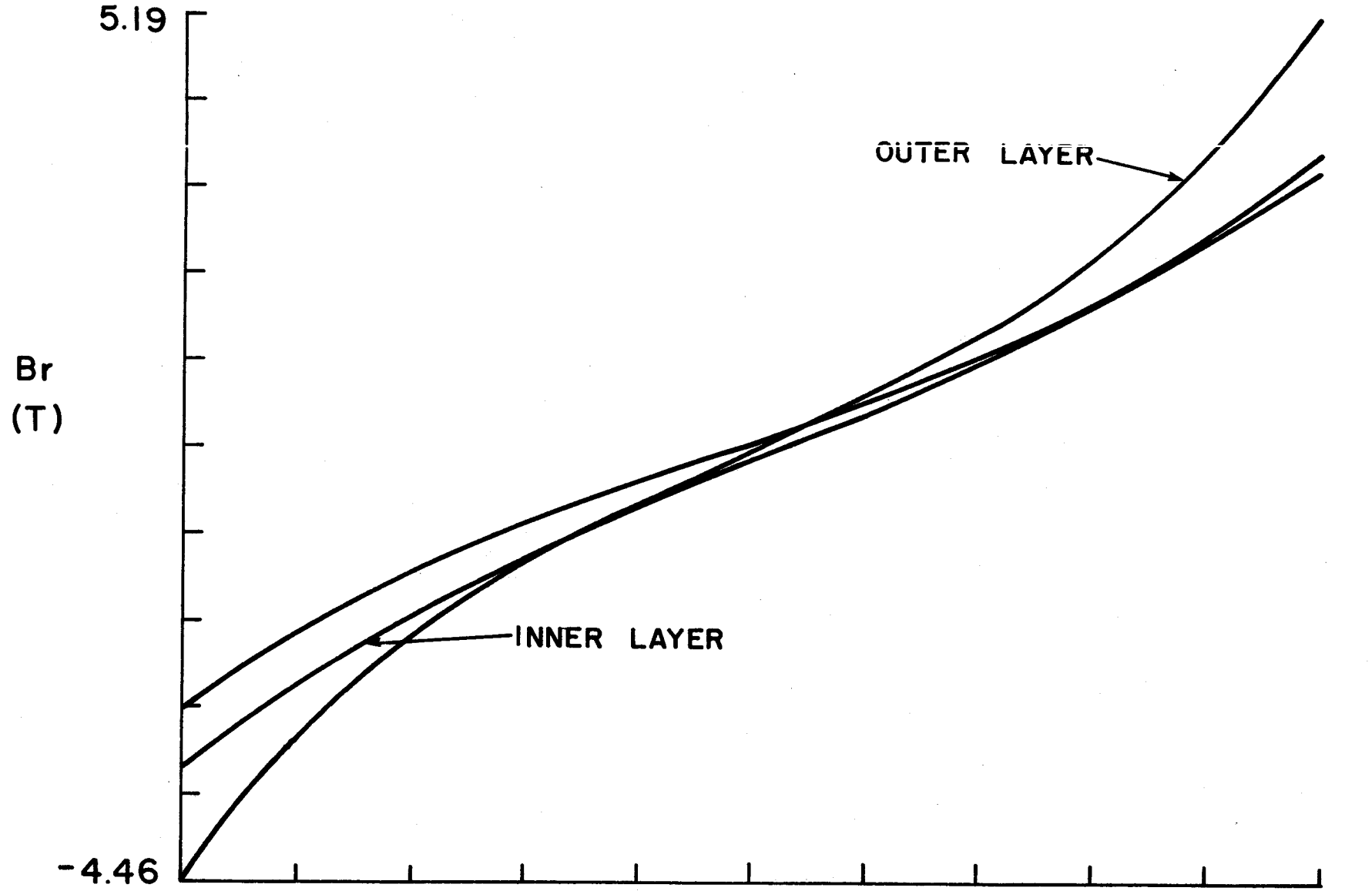

RADIAL FIELD (T) VS. AXIAL POSITION (m)
OF SUPERCONDUCTING CHOKE

FIGURE 27

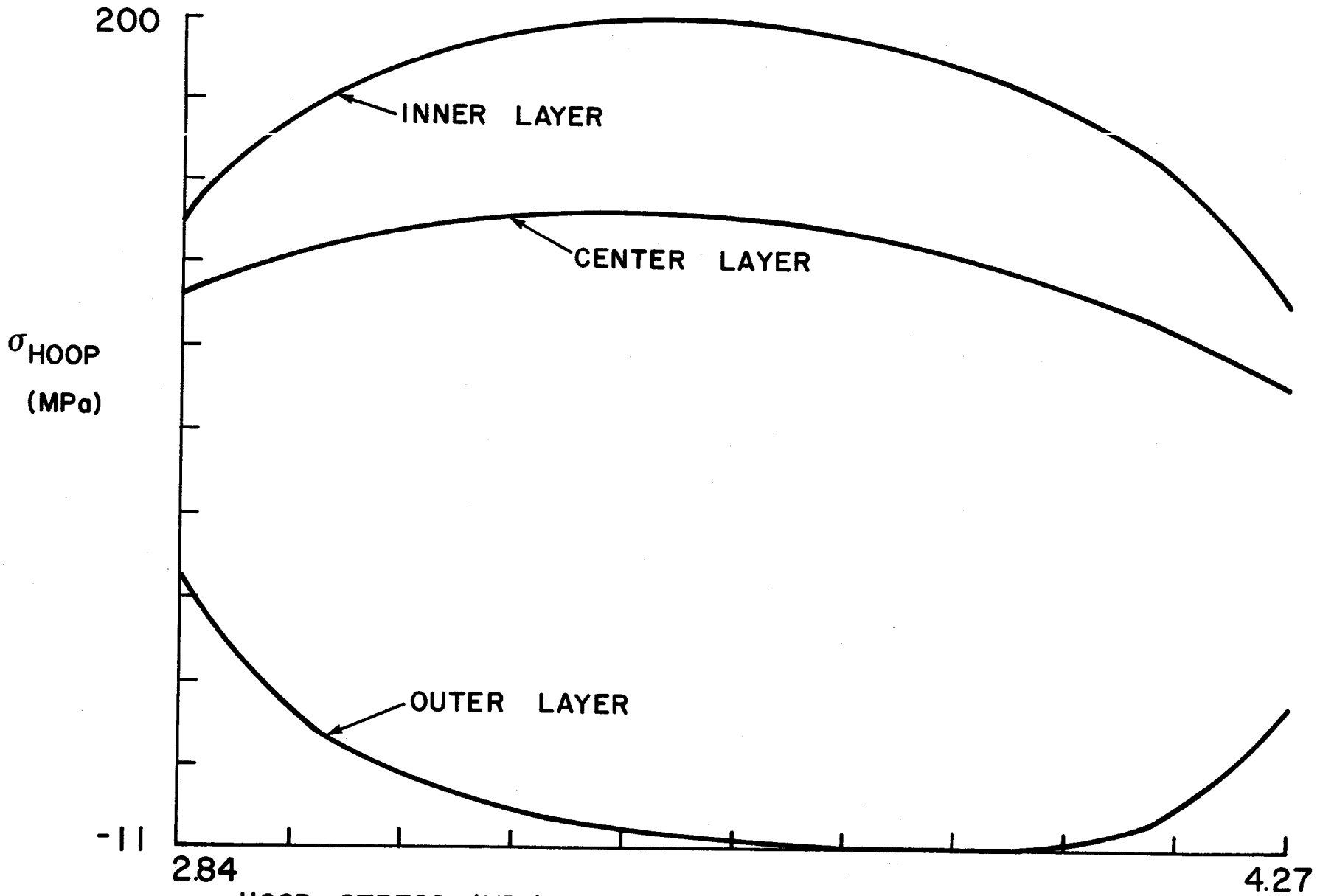

HOOP STRESS (MPa) IN SELF-SUPPORTING SOLENOID CONDUCTORS SUPERCONDUCTING CHOKE, VS. AXIAL POSITION (m)

FIGURE 28

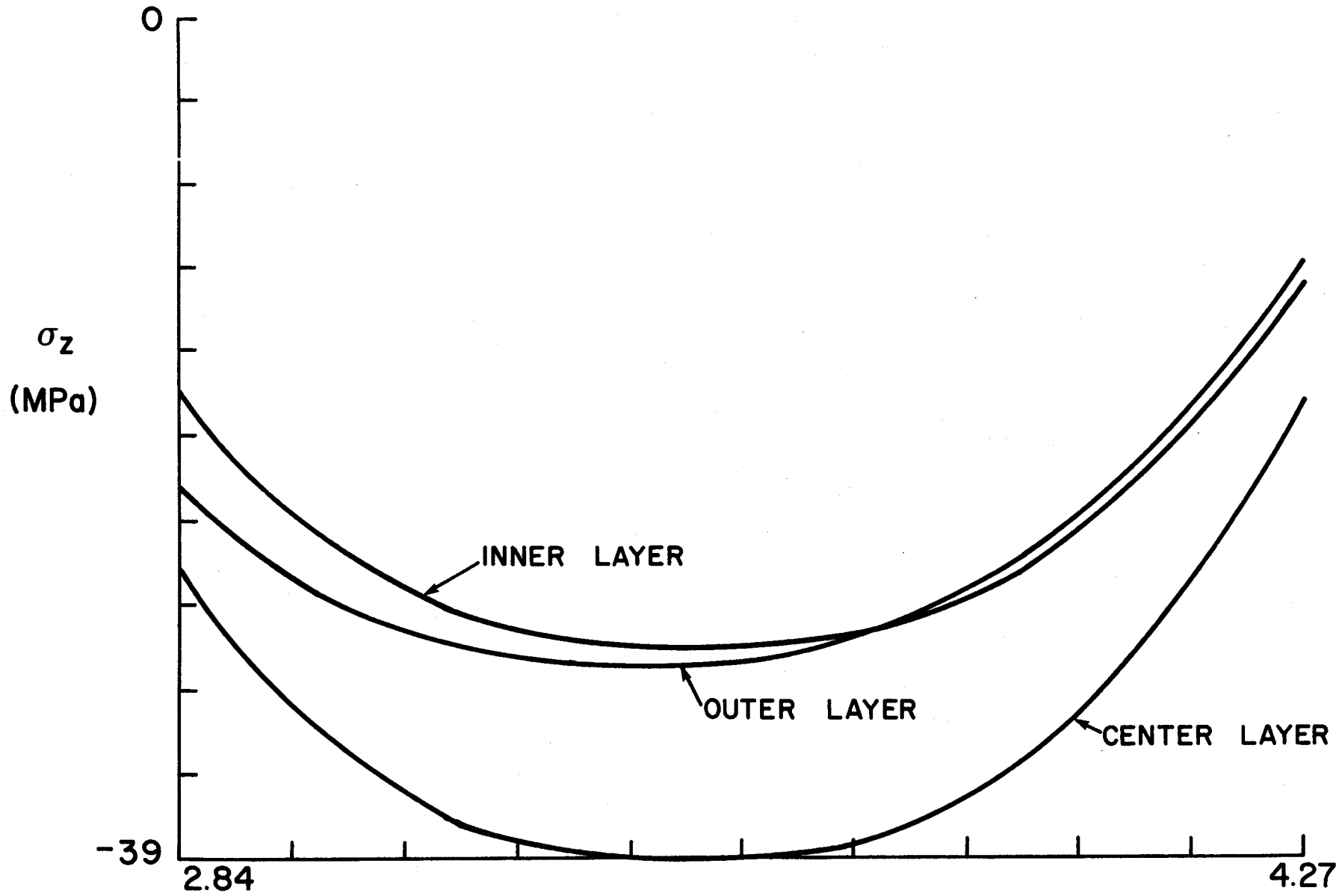

AXIAL STRESSESSES IN A SOLENOID, ASSUMED TO BE SELF-SUPPORTING, (Pa) VS. AXIAL POSITION (m) FOR SUPERCONDUCTING SOLENOID

FIGURE 29

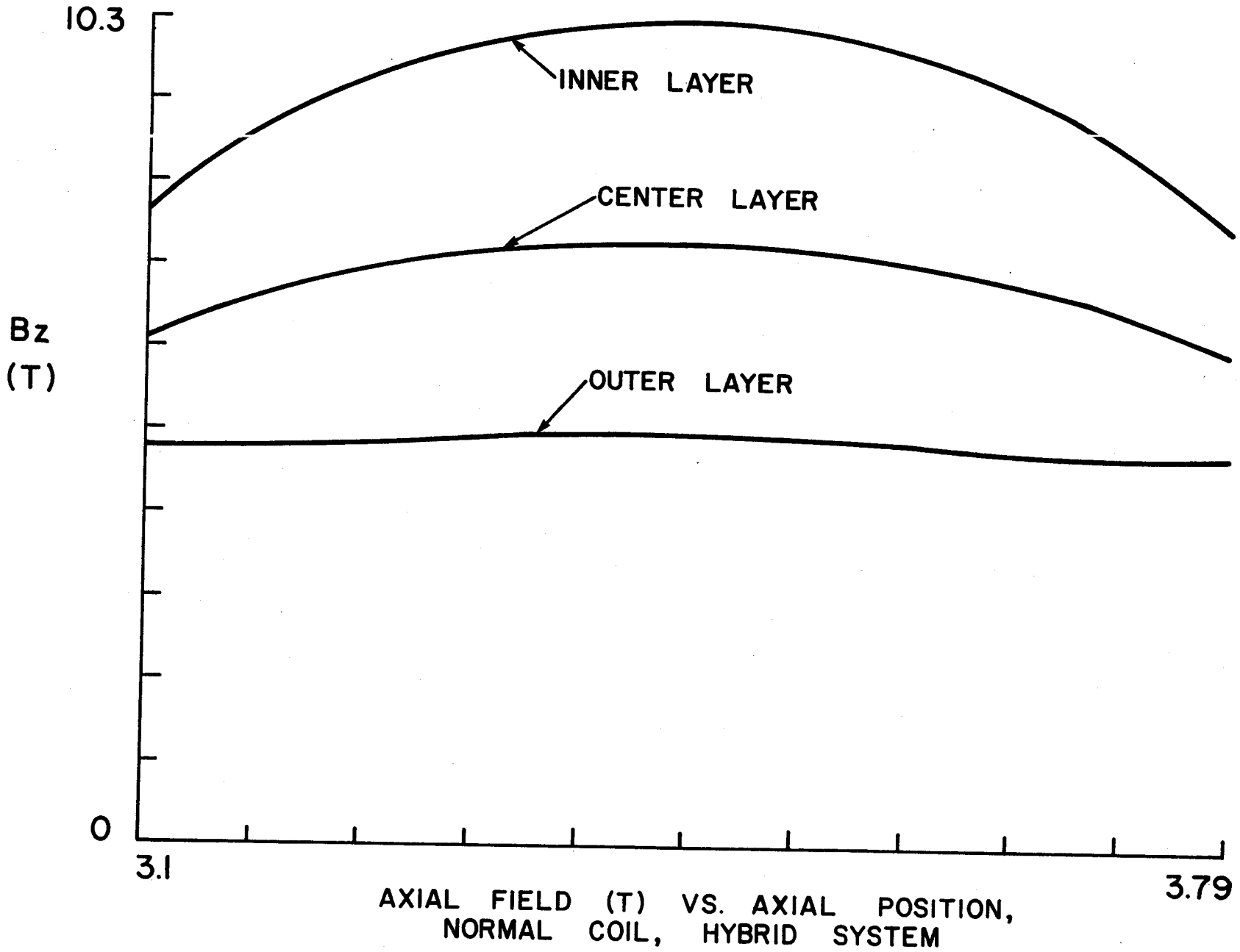

AXIAL FIELD (T) VS. AXIAL POSITION,
NORMAL COIL, HYBRID SYSTEM

FIGURE 30

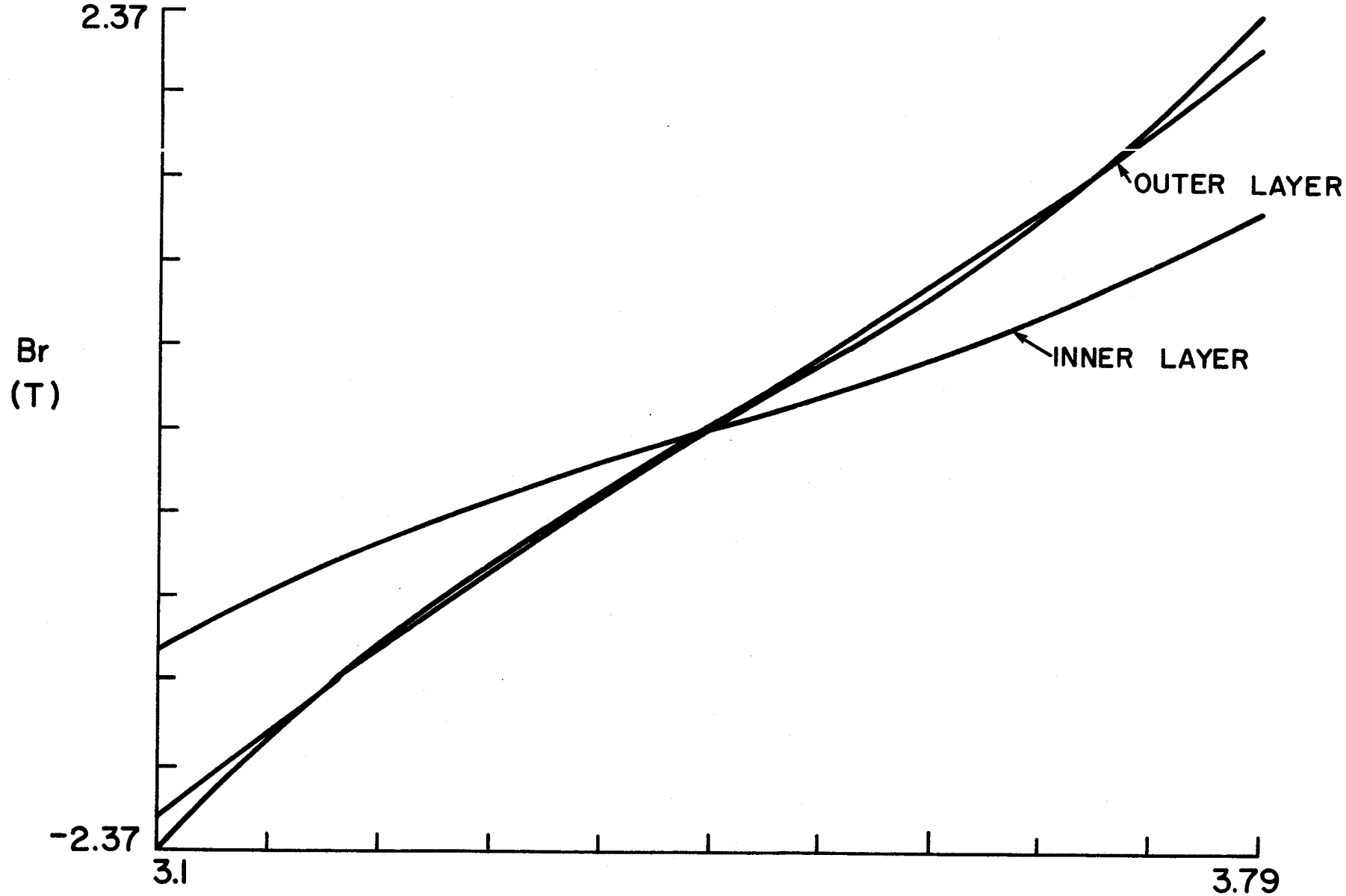

RADIAL FIELD (T) VS. AXIAL POSITION,
NORMAL COIL, HYBRID SYSTEM

FIGURE 31

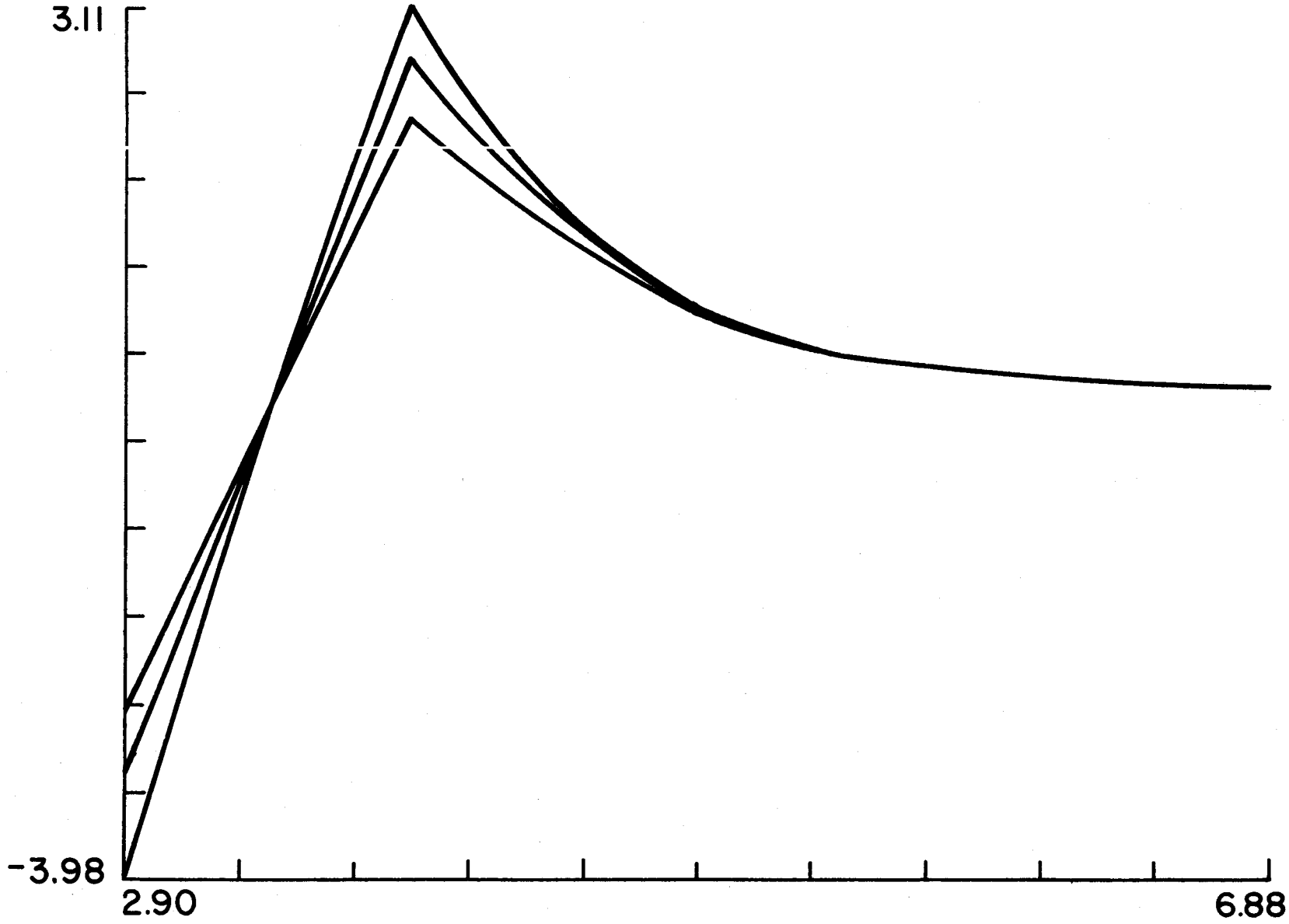

RADIAL FIELD (T) VS. AXIAL POSITION,
SC COIL, HYBRID SYSTEM

FIGURE 32

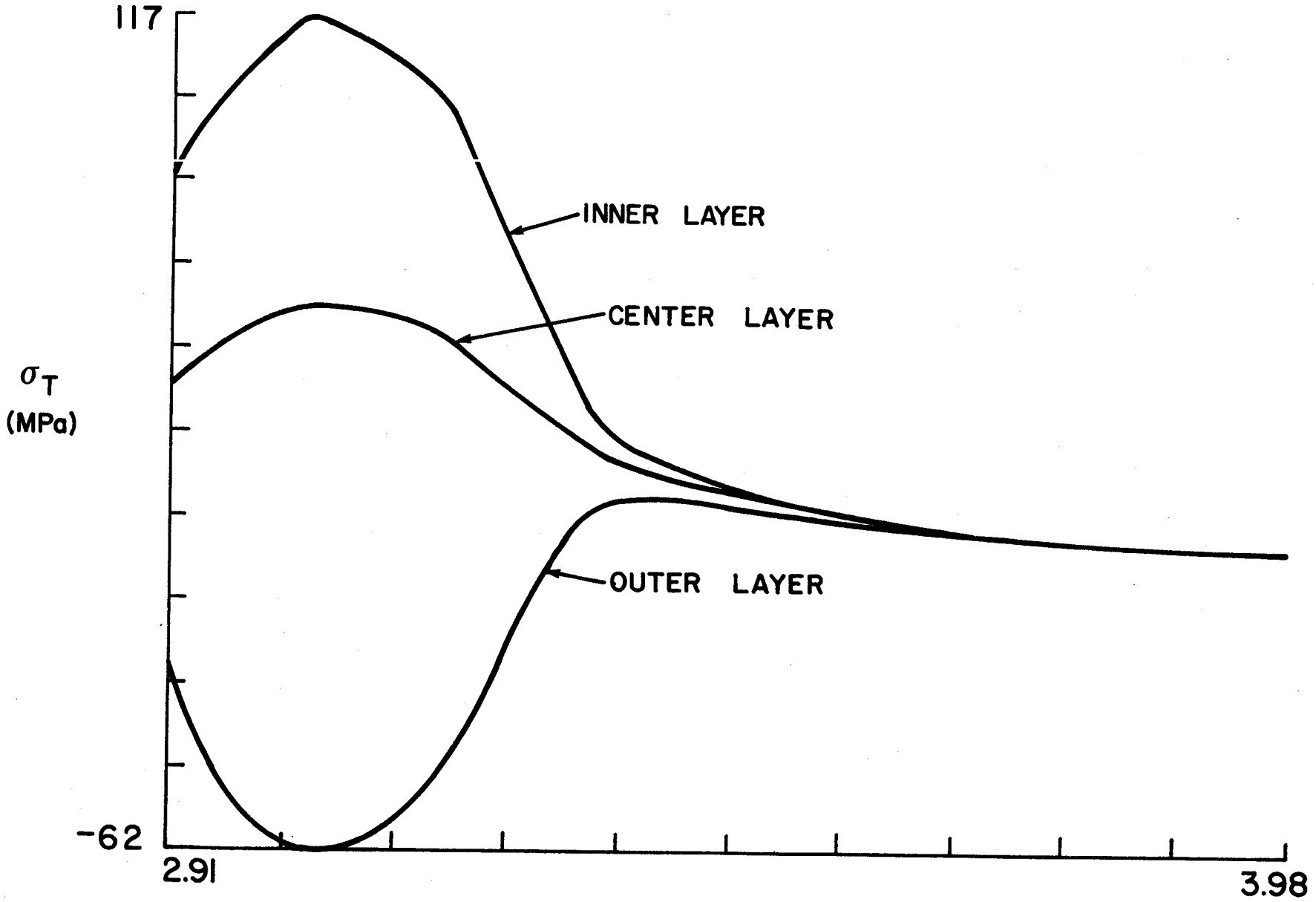

HOOP STRESSES IN SELF-SUPPORTING SOLENOID (Pa) VS. AXIAL POSITION (m) SUPERCONDUCTING MAGNET HYBRID SYSTEM

FIGURE 33

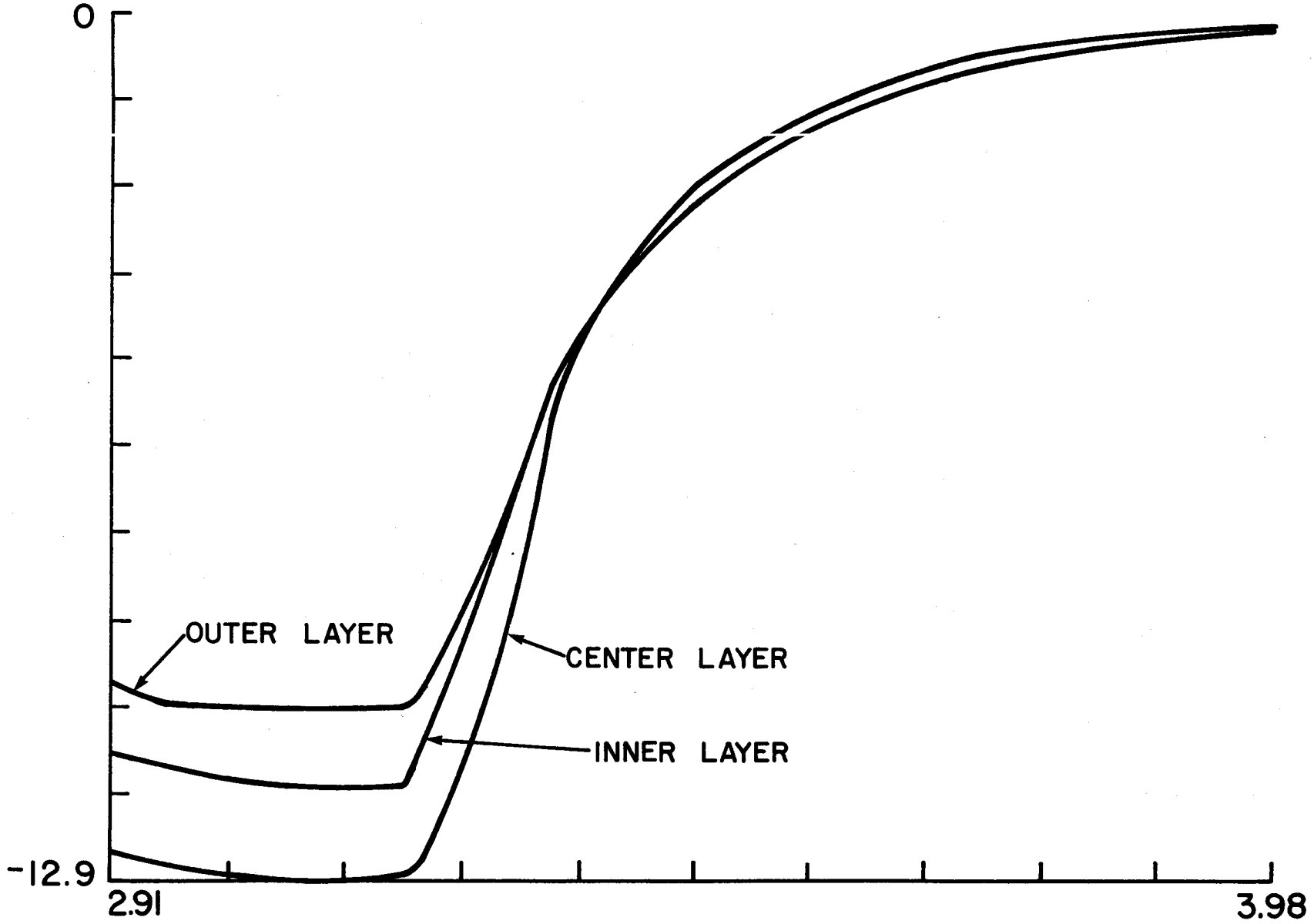

AXIAL STRESSES IN A SOLENOID, ASSUMED TO BE SELF SUPPORTING, (Pa) VS. AXIAL POSITION (m) SUPERCONDUCTING HYBRID SYSTEM

FIGURE 34

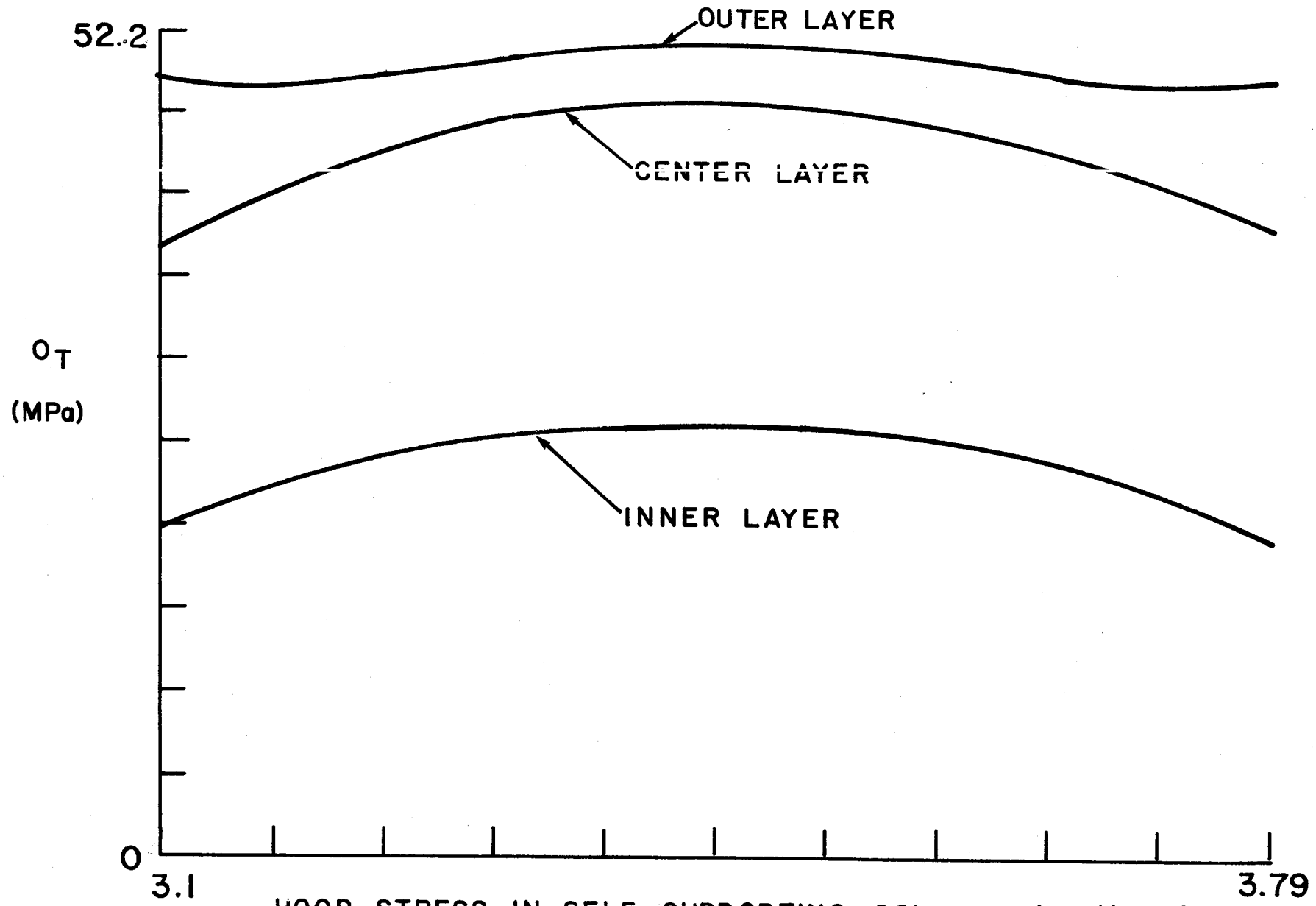

HOOP STRESS IN SELF SUPPORTING SOLENOID (Pa) VS. NORMAL RADIUS (m) NORMAL MAGNET IN HYBRID CHOKE SYSTEM

FIGURE 35

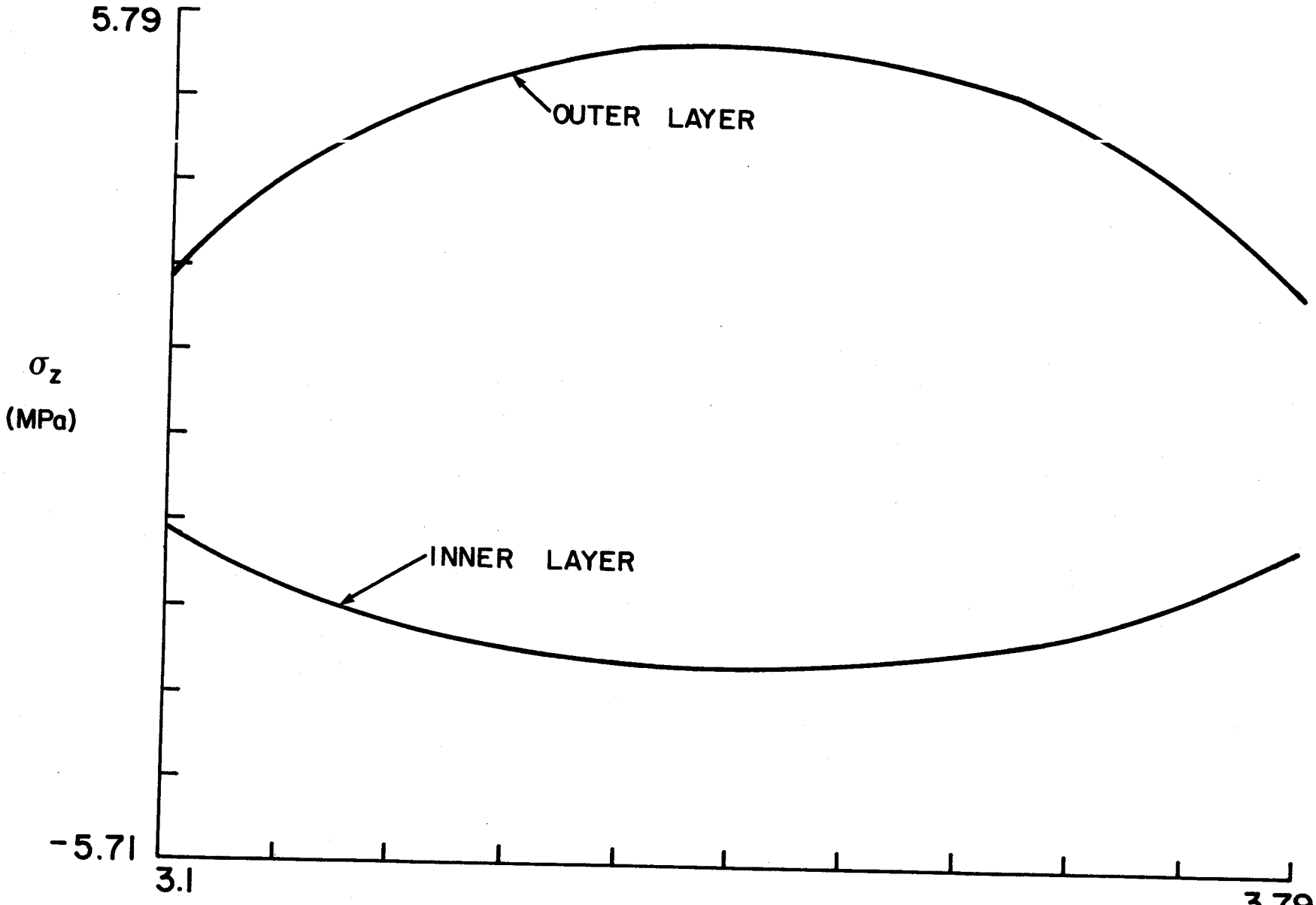

AXIAL STRESSES IN A SOLENOID, (MPa) ASSUMED TO BE SELF-SUPPORTING, VS. NORMAL RADIUS (m) NORMAL MAGNET IN HYBRID CHOKE SYSTEM

FIGURE 36

COST OF THE NEUTRAL BEAM SYSTEM
FOR NORMAL CHOKE COIL

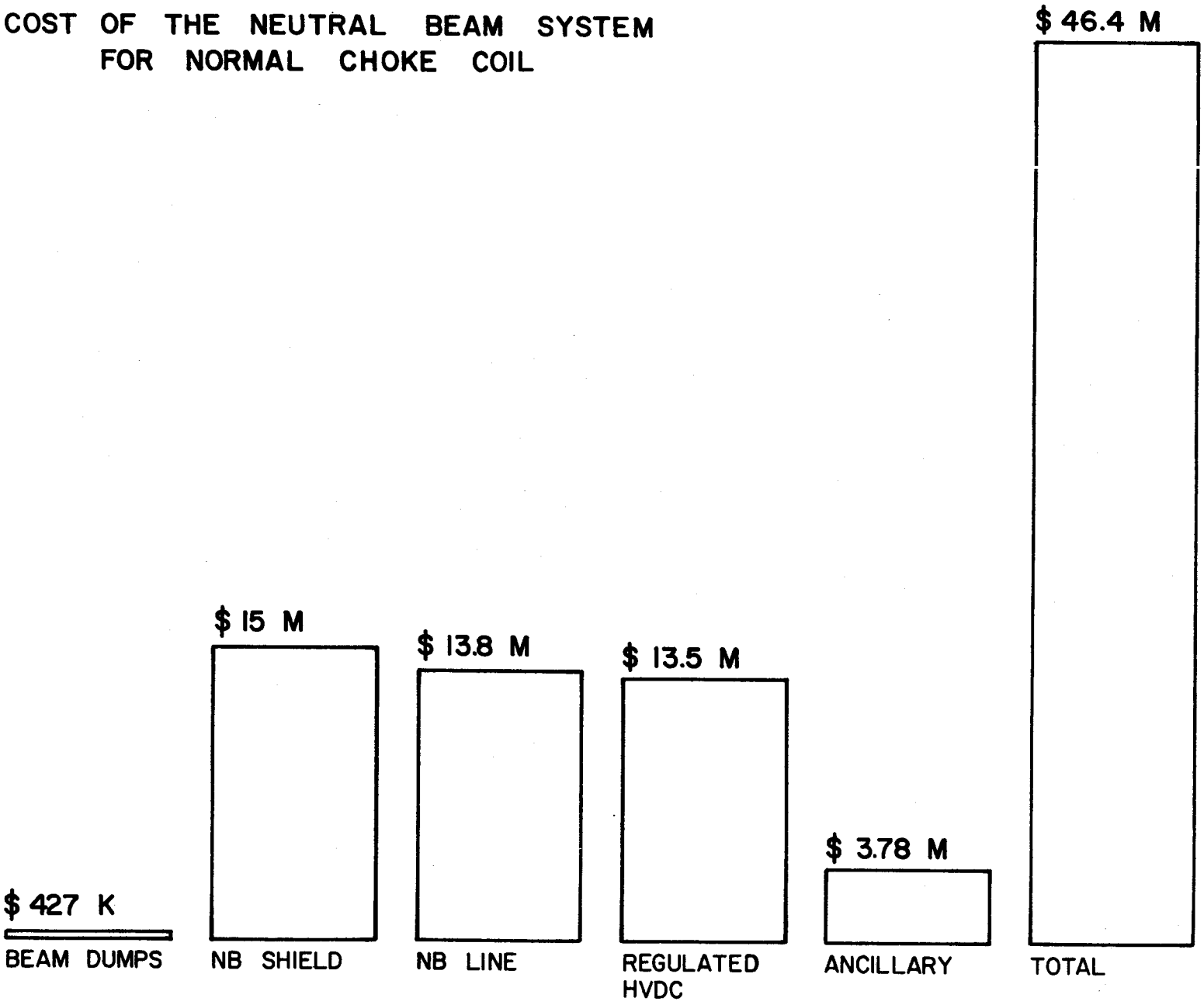

FIGURE 37

COST OF NORMAL CHOKE MAGNET AND AUXILIARY EQUIPMENT

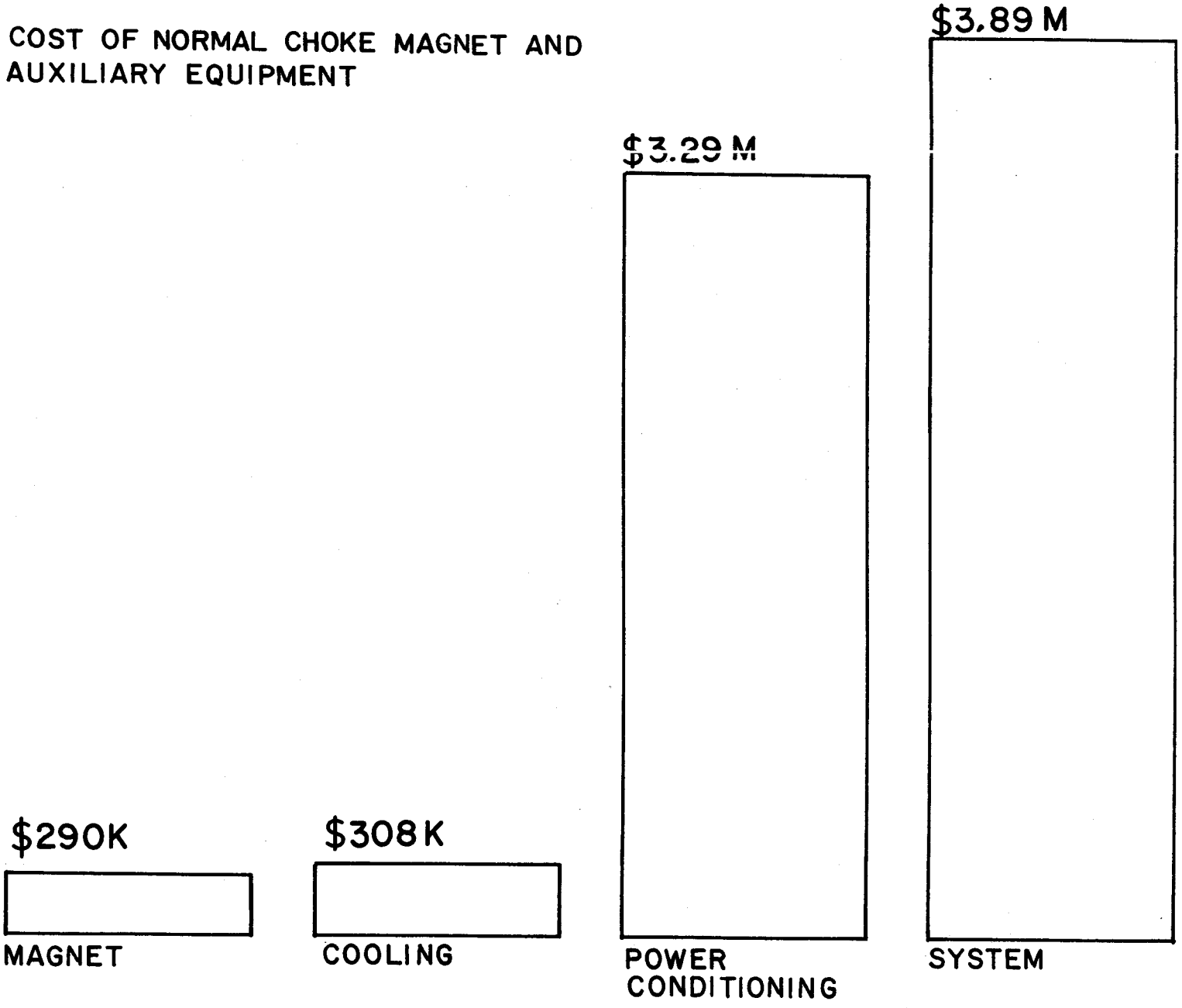

FIGURE 38

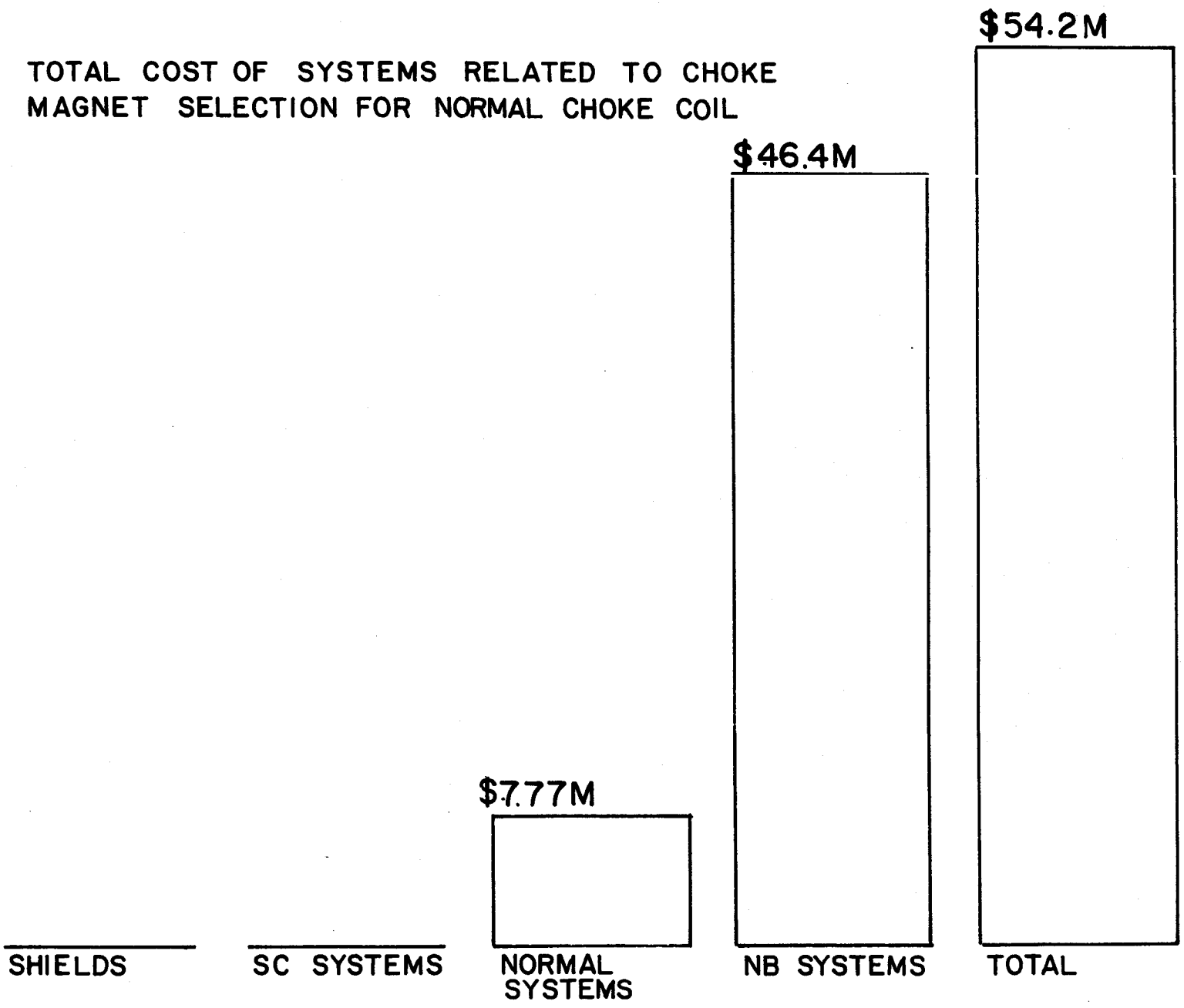
TOTAL COST OF SYSTEMS RELATED TO CHOKE MAGNET SELECTION FOR NORMAL CHOKE COIL
$54.2M
$46.4M
$7.77M
SHIELDS
SC SYSTEMS
NORMAL SYSTEMS
NB SYSTEMS
TOTAL

FIGURE 39

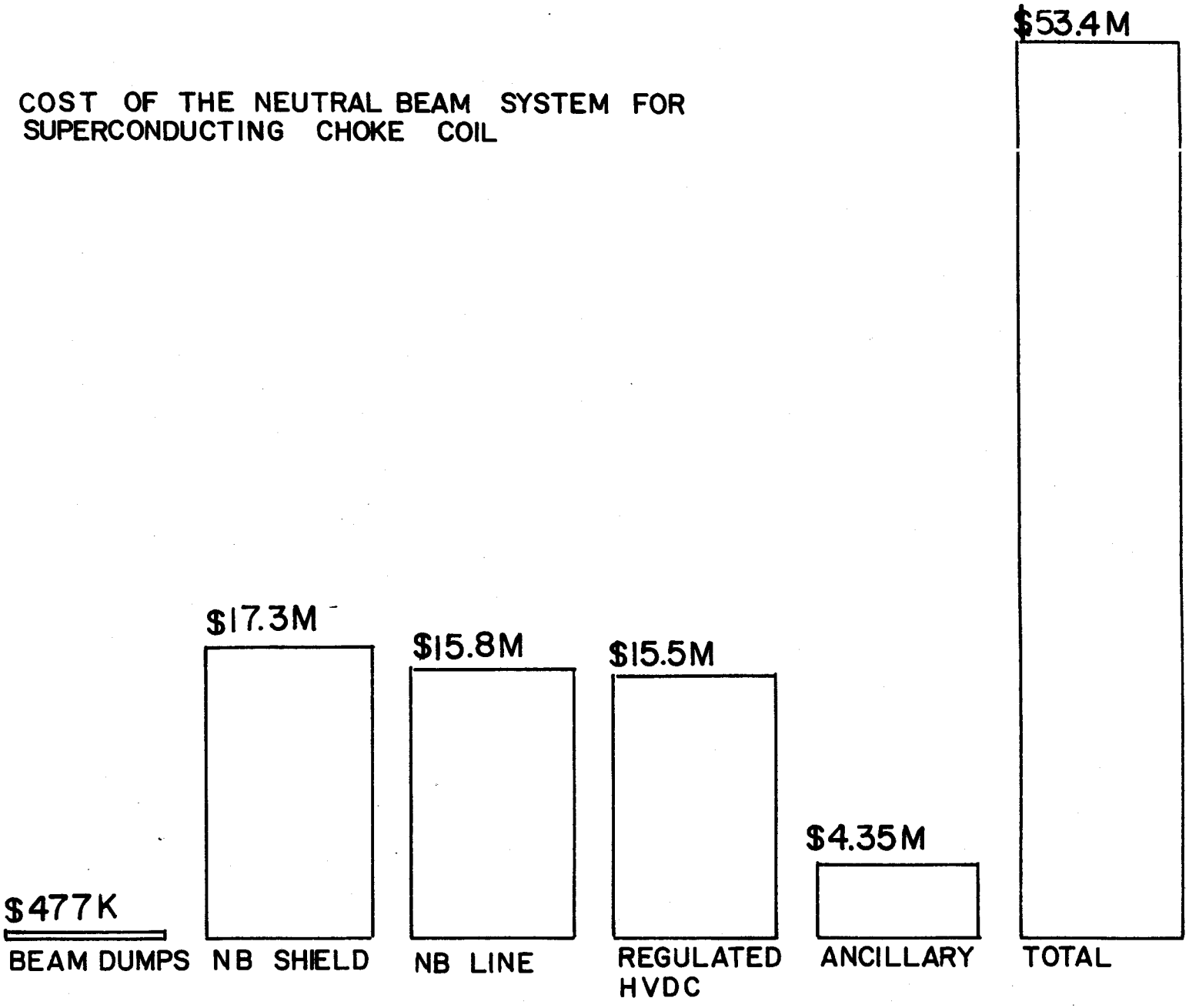
COST OF THE NEUTRAL BEAM SYSTEM FOR SUPERCONDUCTING CHOKE COIL
$53.4M
$17.3M
$15.8M
$15.5M
$4.35M
$477K
BEAM DUMPS
NB SHIELD
NB LINE
REGULATED HVDC
ANCILLARY
TOTAL

FIGURE 40

COST OF A SUPERCONDUCTING CHOKE COIL AND AUXILIARY EQUIPMENT

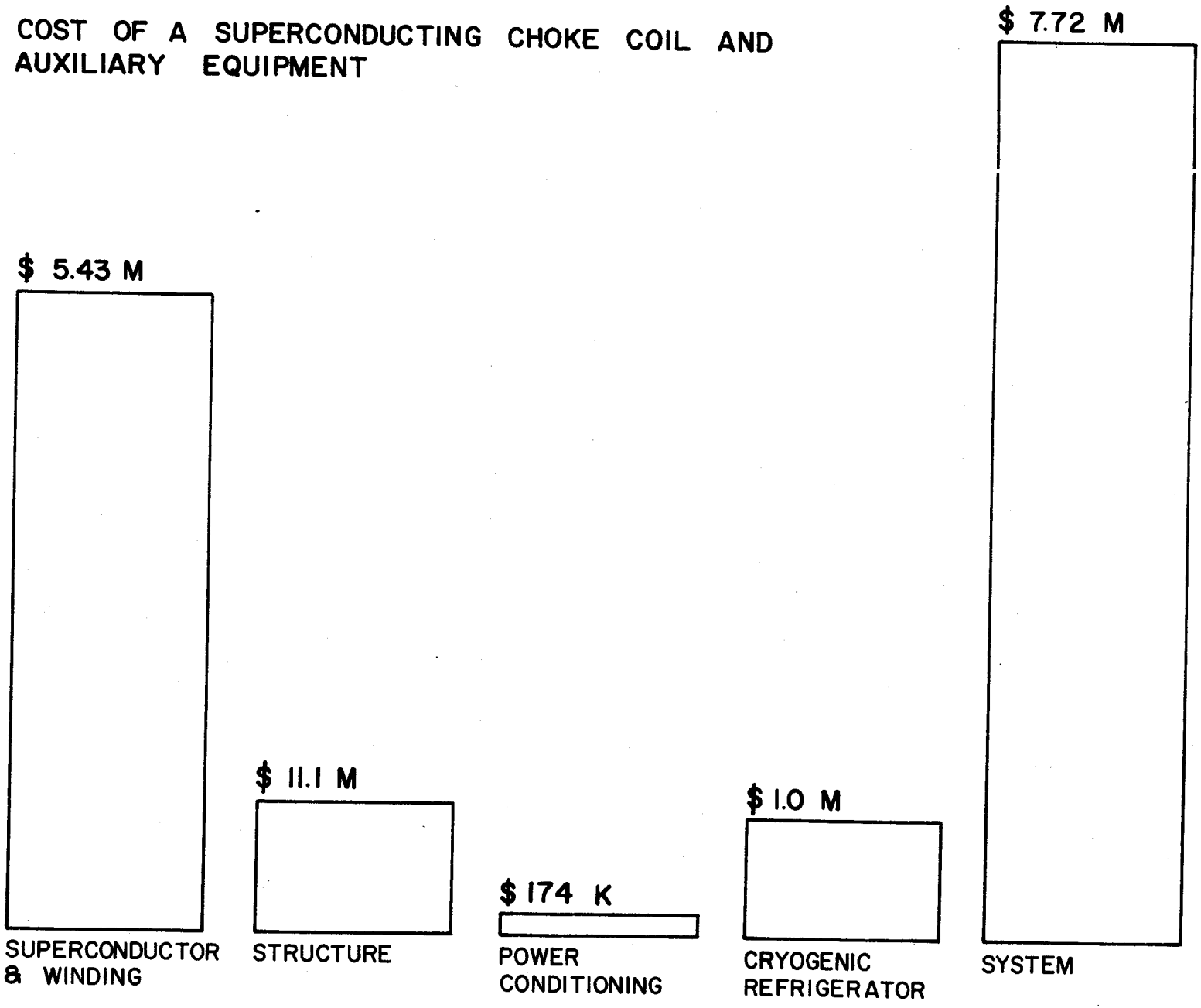

FIGURE 41

TOTAL COST OF SYSTEMS RELATED TO CHOKE MAGNET FOR SUPERCONDUCTING CHOKE SYSTEM

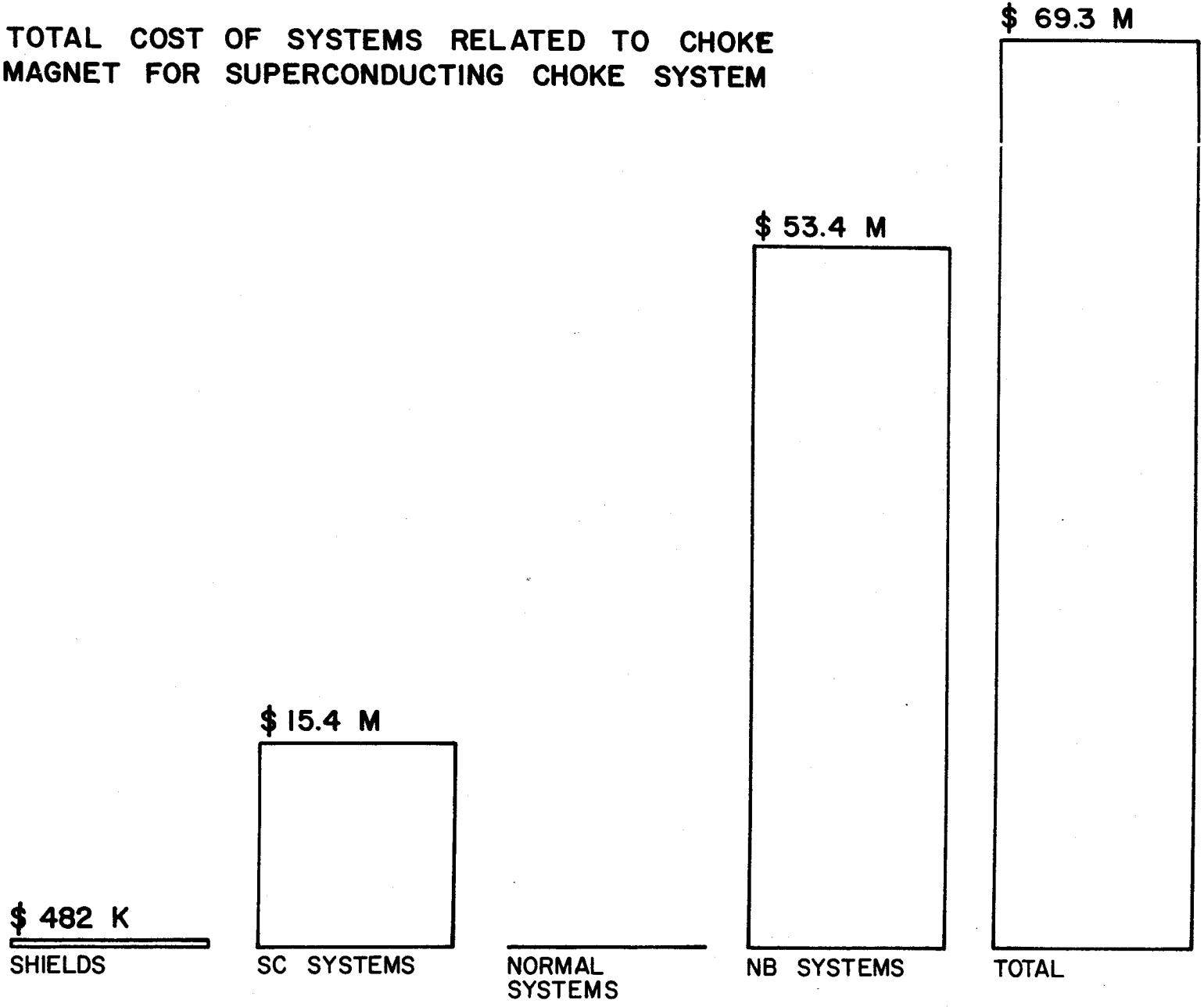

FIGURE 42

COST OF THE NEUTRAL BEAM SYSTEM WITH HYBRID CHOKE

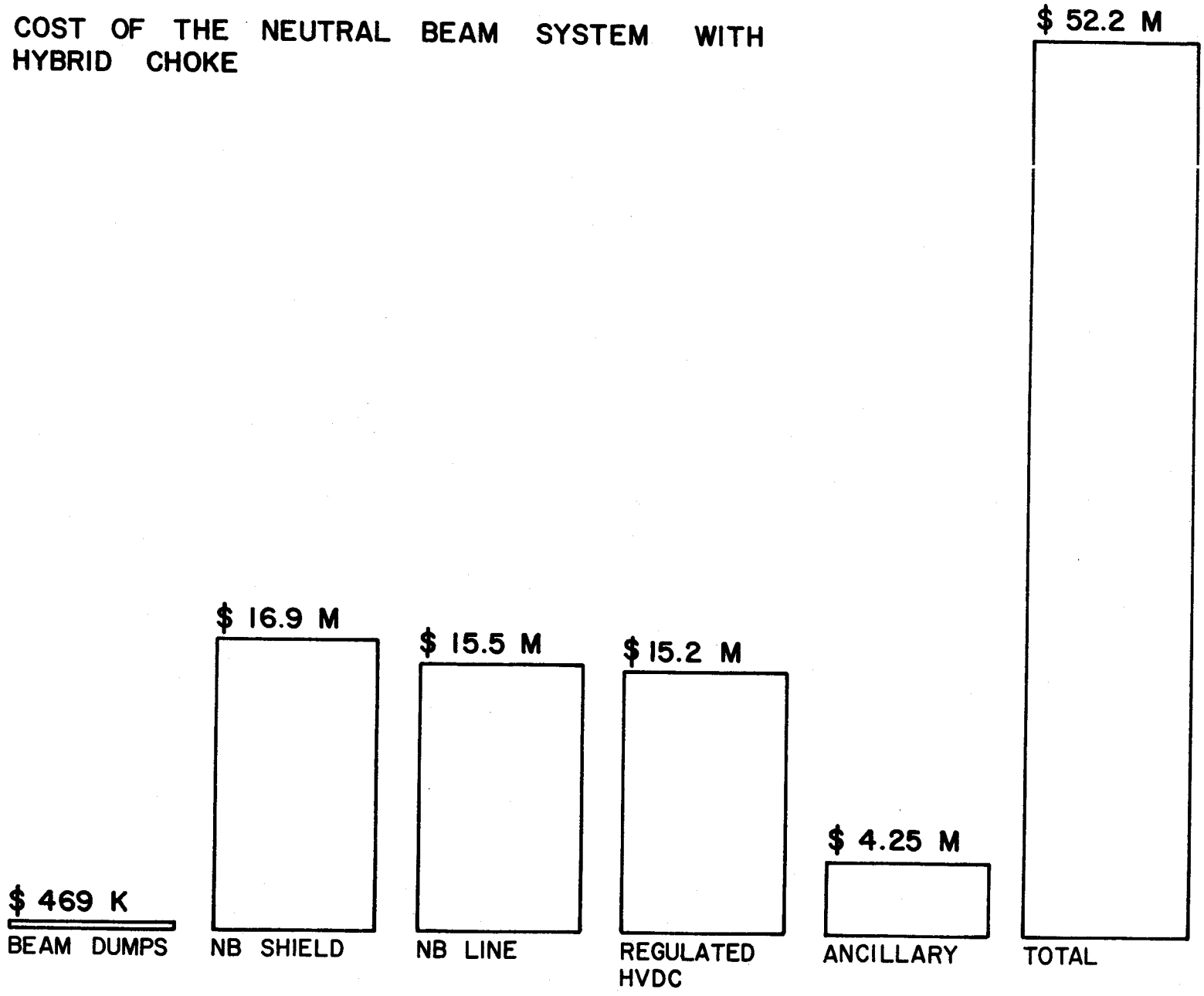

FIGURE 43

COST OF A NORMAL CHOKE MAGNET AND AUXILIARY EQUIPMENT IN HYBRID CHOKE SYSTEM

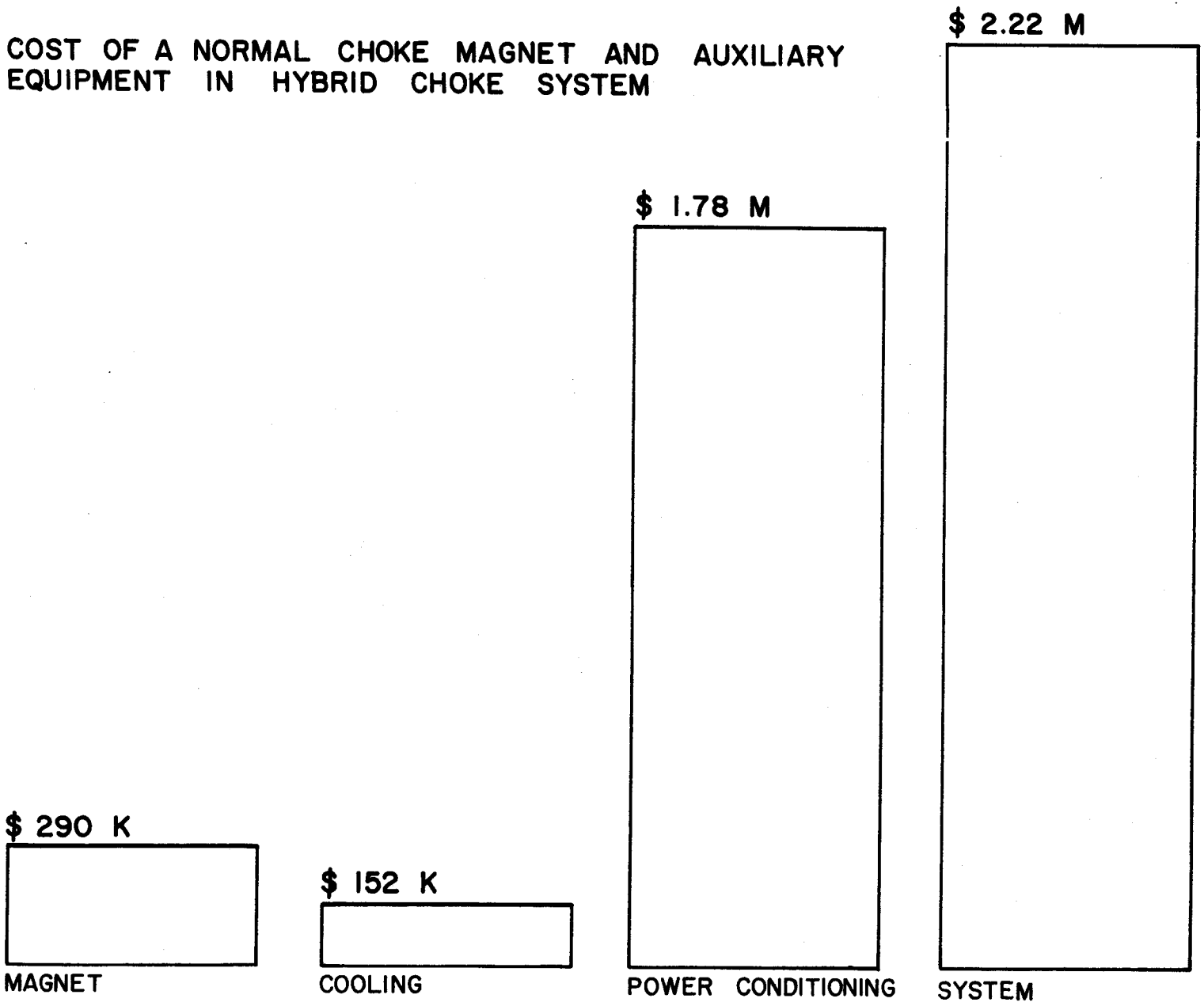

FIGURE 44

COST OF A SUPERCONDUCTING CHOKE COIL AND AUXILIARY EQUIPMENT IN HYBRID CHOKE SYSTEM

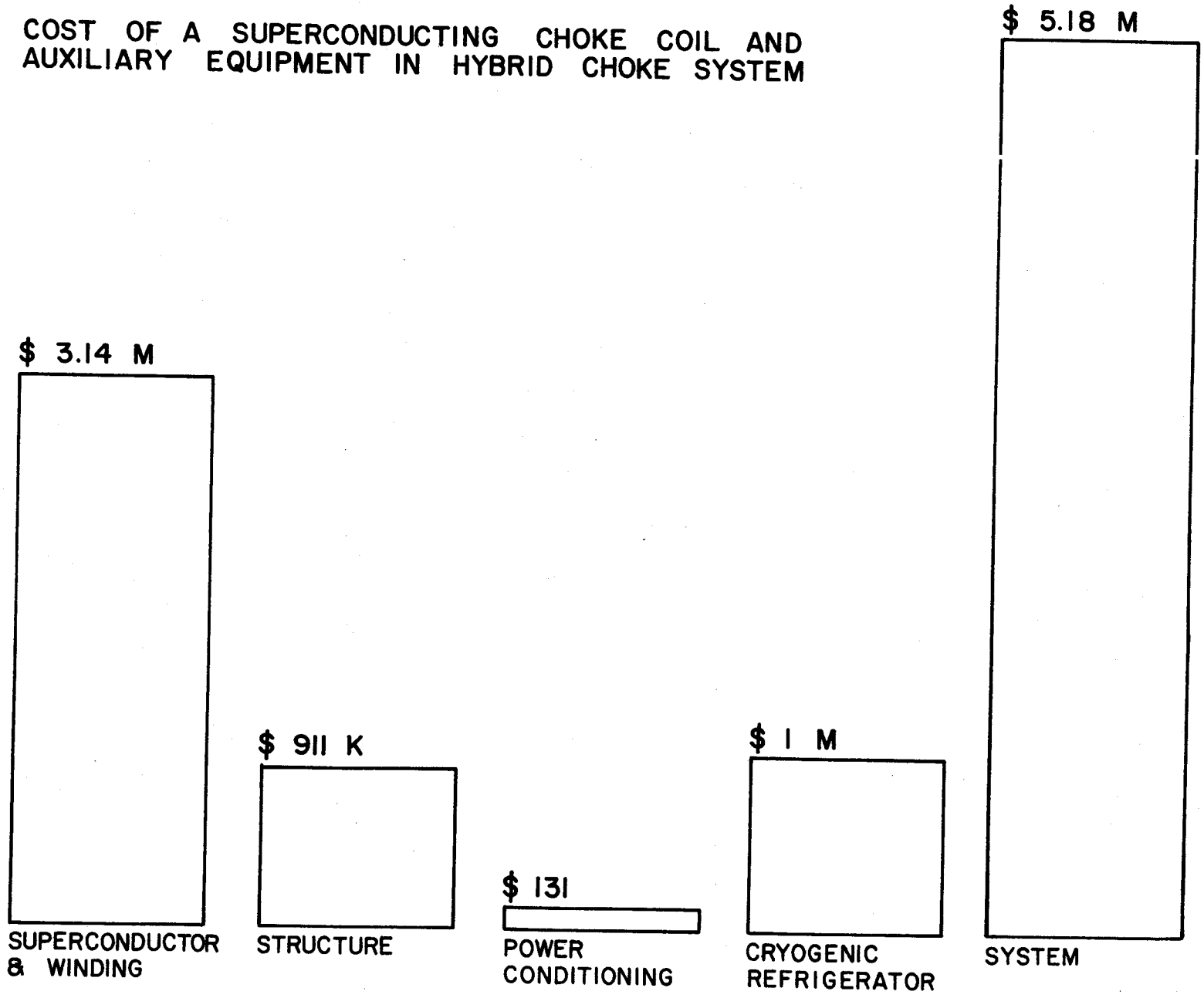

FIGURE 45

TOTAL COST OF SYSTEMS RELATED TO CHOKE MAGNET SELECTION IN HYBRID CHOKE MAGNET SYSTEM

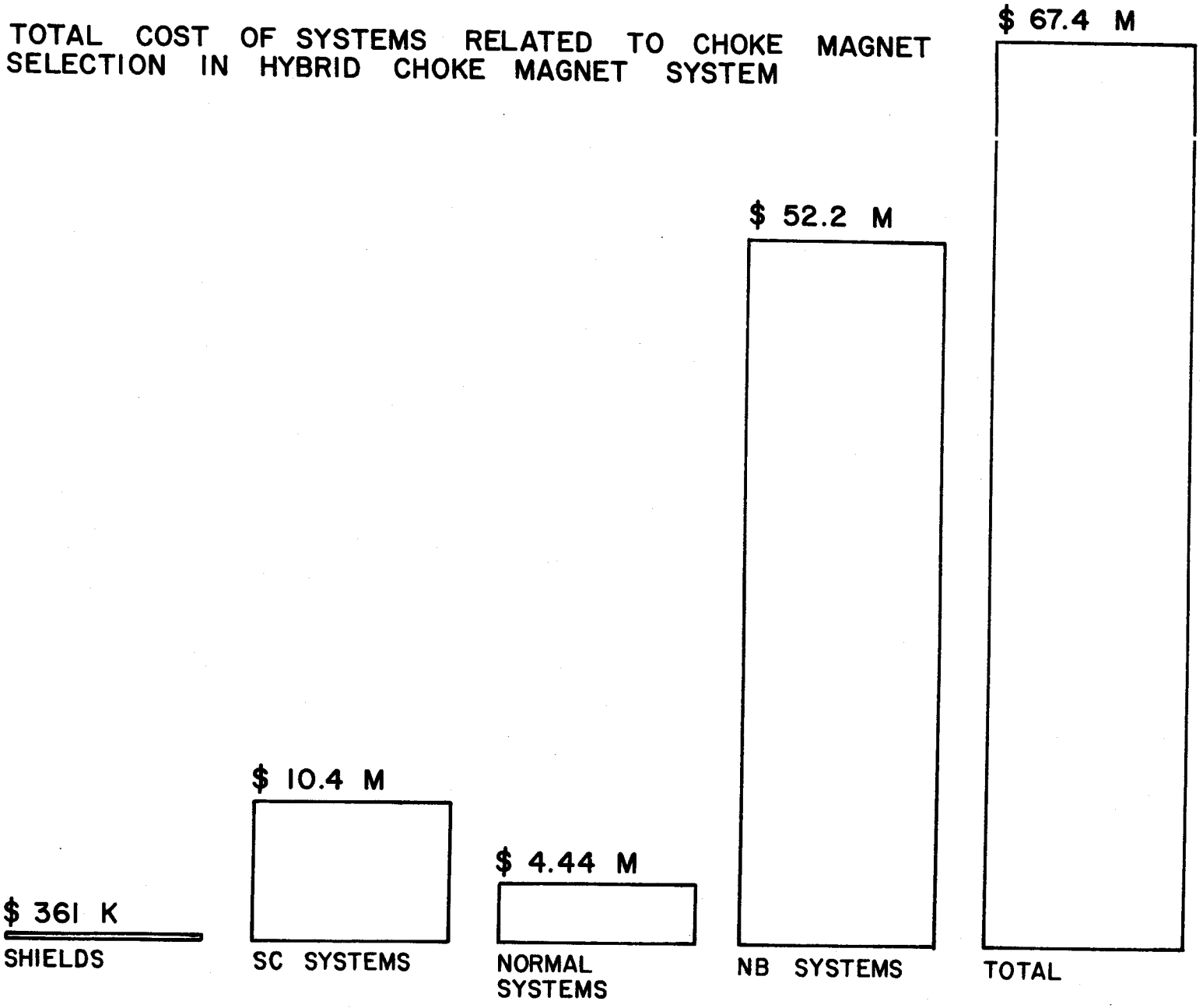

MIT PLASMA FUSION CENTER TECHNOLOGY DISTRIBUTION LIST

AEB, Plasma Physics Division, South Africa, De Villiers, Johan
AMPC Inc., Guest, Dr. G.
Association Euratom - CEA, Dept. de Physique de Plasma et de la Fusion Controle, France
Australian National University, Australia, Hamberger, S.M.
Bank of Tokyo, Ltd., Japan, Azuma, Mr. Katsuhiko
Brookhaven National Labora ory, Powell, James R.
Central Research Institute for Physics, Hungary, Kostka, P.
Chalmers University of Technology, Sweden, Wilhelmsson, K.H.B.
CNEN - Centro di Frascati, Italy
CNR - Centro di Studio sui Gas Ionizzati, Italy, Ortolani, S.
Consoli, T., France
Culham Laboratory, United Kingdom, Wesson, J.A.
Division of Research and Laboratories, Austria, Frolov, V.
Ecole Royale Militaire, Belgium, Vandenplas, P.E.
EG&G Idaho, Inc., Crocker, Mr. J.
Electrical Power Research Institute, Ambeard, Dr. Noel
FOM-Institute for Plasma Physics, Rijnhuizen, Netherlands
General Atomic Company
Georgia Institute of Technology, Stacey, Jr., Dr. W.M.
ITT, India, Tewari, Prof. D.P.
Inst. of Physics, Warsaw University Branch, Poland, Brzosko, J.S.
Inst. Nacional de Invest. Nucleares, Mexico, Ramos Salas, J.S.
Japan Atomic Energy Research Institute, Japan, Mori, Dr. S.
JET Joint Undertaking, United Kingdom
KFA Julich, Institut fur Plasmaphysik, FRG
Kurchatov Institute of Atomic Energy, USSR
Lawrence Berkeley Laboratory, Sessler, Dr. A.M.
Lawrence Livermore Laboratory, Alira, Richard
Lebedev Institute of Physics, USSR, Rabinovich, Dr. M.S.
Los Alamos Scientific Laboratory, CTR Division
Max-Planck-Institute fur Plasmaphysik, FRG
Naval Research Laboratory, Granatstein, Dr. Victor
New York University, Courant Inst. of Mathematical Sci., Grad, Prof H.
Nuclear Research Institute, Czechoslovakia, Bartosek, V.
Oak Ridge National Laboratory, Fusion Energy Division
Oak Ridge National Laboratory, Peng, Y-K. M.
Osaka University, Japan, Ito, H.
Palumbo, D., Belgium
Princeton University, Princeton Plasma Physics Laboratory
Rijksuniversiteit Gent, Belgium, Verheest, F.
Riso National Laboratory, Denmark, Jensen, V.O.
Royal Institute of Technology, Sweden, Lehnert, B.P.
Ruhr-Universitat, FRG, H-J. Kunze
S. Kaliski Inst. of Plasma Phys. and Laser Microfusion, Poland, Fiedorowicz, H
Sandia Research Laboratories, Yonas, Dr. Jerry
Science Applications, Inc., MD, Dean, Dr. Stephen
Science Council of Japan, Japan, Fushimi, K.
Siberian Section of the USSR Academy of Sciences, USSR, Ryutov, Dr. D.D.
Soreq Nuclear Research Center, Israel, Rosenblum, M.
Stanford University, Bunemar, Prof. O.
Technion, Israel, Rosenau, P.
Tel-Aviv University, Israel, Cuperman, S.
TRW Defense and Space Systems, Lazar, Dr. Norman
U.S. Department of Energy, Office of Fusion Energy
U.S. Department of Energy, Kostoff, Dr. Ronald N.
U.S. Department of Energy, Thomasson, Dr. Neil
U.S. Department of Energy, Trivelpiece, Dr. A.W.
Universitat Innsbruck, Austria, Cap, F.
Universitat Stuttgart, FRG, Wilhelm, R.
Universite de Montreal, Canada, Paquette, G.
Universite Libre de Bruxelles, Belgium, Balescu, R.C.
University of Alberta, Canada, Offenberger, A.A.
University of Bergen, Norway, G. Berge
University of British Columbia, Canada, Curzon, Dr. F.
University of California at Berkeley, Kunkel, Prof. W.
University of California at Berkeley, Lichtenberg, Prof. A.
University of California at Irvine
University of California at L.A., Dept. of Engineering Science
University of California at San Diego, Dept. of Physics
University of Malay, Malaysia, Lee, S.
University of Maryland, Department of Physics
University of Nairobi, Kenya, Malo, J.O.
University of Natal, South Africa, Hellberg, M.A.
University of Rochester, Simon, Prof. Albert
University of Saskatchewan, Canada, Hirose, A.
University of Texas, Dept. of Physics
University of Texas, Kochanski, Dr. Ted
University of Waikato, New Zealand, Hosking, R.J.
University of Washington, Vlases, Dr. George
University of Wisconsin:
    Department of Physics
    Nuclear Engineering Department
Varian
Yale University, Hirshfield, Prof. J.

PFC BASE MAILING LIST

Argonne National Laboratory, TIS, Reports Section
Associazione EURATOM - CNEN Fusione, Italy, The Librarian
Battelle-Pacific Northwest Laboratory, Technical Info Center
Brookhaven National Laboratory, Research Library
Central Research Institute for Physics, Hungary, Preprint Library
Chinese Academy of Sciences, China, The Library
The Flinders University of S.A., Australia, Jones, Prof. I.R.
General Atomic Co., Library
General Atomic Co., Overskei, Dr. D.
International Atomic Energy Agency, Austria,
Israel Atomic Energy Commission, Soreq Nucl. Res. Ctr., Israel
Kernforschungsanlage Julich, FRG, Zentralbibliothek
Kyushu University, Japan, Library
Lawrence Berkeley Laboratory, Library
Lawrence Livermore Laborary, Technical Info Center
Max-Planck-Institut fur Plasma Physik, FRG, Main Library
Nagoya University, Institute of Plasma Physics, Japan
Oak Ridge National Laboratory, Fusion Energy Div. Library
Oak Ridge National Laboratory, Derby, Roger

Physical Research Laboratory, India, Sen, Dr. Abhijit
Princeton University, PPL Library
Rensselaer Polytechnic Institute, Plasma Dynamics Lab.
South African Atomic Energy Board, S. Africa, Hayzen, Dr. A.
UKAEA, Culham Laboratory, United Kingdom, Librarian
US Department of Energy, DOE Library
Universite de Montreal, Lab. de Physique des Plasmas, Canada
University of Innsbruck, Inst. of Theoretical Physics, Austria
University of Saskatchewan, Plasma Physics Lab., Canada
University of Sydney, Wills Plasma Physics Dept., Australia
University of Texas at Austin, Fusion Res. Ctr., Library
University of Wisconsin, Nucl. Eng. Dept., UW Fusion Library

INTERNAL MAILINGS

MIT Libraries
Industrial Liaison Office
G. Bekefi, A. Bers, D. Cohn, B. Coppi, R.C. Davidson,
T. Dupree, S. Foner, J. Freidberg, M.O. Hoenig, M. Kazimi,
L. Lidsky, E. Marmar, J. McCune, J. Meyer, D.B. Montgomery,
J. Moses, D. Pappas, R.R. Parker, N.T. Pierce, P. Politzer,
M. Porkolab, R. Post, H. Praddaude, D. Rose, J.C. Rose,
R.M. Rose, B.B. Schwartz, L.D. Smullin, R. Temkin, P. Wolff,
T-F. Yang